SIMULATION OF ICESAT/GLAS FULL-WAVEFORM OVER HIGHLY RUGGED TERRAIN

Girish Kumar Yadav

January, 2010

Simulation of ICESat/GLAS Full -waveform over Highly Rugged Terrain

by

Girish Kumar Yadav

Thesis submitted to the International Institute for Geo-information Science and Earth Observation (The Netherlands) and Indian Institute of Remote Sensing (Dehradun, India) in partial fulfilment of the requirements for the degree of Master of Science in Geo-information Science and Earth Observation, Specialisation: (Geo-informatics).

Thesis Assessment Board

Chairman:	Prof. Dr. V.G. Jetten
External Expert :	PVSSN Gopala Krishna (NRSC)
ITC Member :	Dr. Nicholas Hamm
IIRS Member :	Mrs. Shefali Agarwal
	Dr. R. S. Chatterjee
	Mr. P. L. N. Raju
	Dr. Sameer Saran

Thesis Supervisor

IIRS :	Mrs. Shefali Agarwal
	Dr. R. S. Chatterjee
ITC :	Dr. Martin Rutzinger

INTERNATIONAL INSTITUTE FOR GEO-INFORMATION SCIENCE AND EARTH OBSERVATION (ITC), FACULTY OF UNIVERSITY OF TWENTE
ENSCHEDE, THE NETHERLANDS

&

INDIAN INSTITUTE OF REMOTE SENSING (IIRS), NATIONAL REMOTE SENSING CENTRE (NRSC)
DEPARTMENT OF SPACE, GOVT. OF INDIA
DEHRADUN, INDIA

Disclaimer

This document describes work undertaken as part of a programme of study at the International Institute for Geo-information Science and Earth Observation. All views and opinions expressed therein remain the sole responsibility of the author, and do not necessarily represent those of the institute.

Dedicated to

My Family & Friends

Abstract

Spaceborne laser altimetry has proved to be very useful tool to measure and monitor earth surface and to estimate biophysical parameters of forest. ICESat is the one and only spaceborne laser altimetry satellite. It provides full-waveform laser altimetry data globally with approximately 70 m footprint on ground. Full-waveform represents the sampling of digitized backscattered laser energy in 1 ns time interval. Full-waveform represents the vertical distribution of within footprint illuminated surface and objects, with very high vertical resolution of 15 cm. Due to ICESat's high resolution vertical profiling and vegetation penetration abilities, laser full-waveforms provide good estimation of biophysical parameters over flat terrain. Over rugged terrain nature of full-waveform becomes complex, due to the mixing of canopy and ground signals.

In this research a full-waveform simulation algorithm is developed to understand the characteristics and behaviour of ICESat full-waveform vis-à-vis terrain relief. Waveforms are analyzed over terrain with different ruggedness. Highly rugged ravine topography of Chambal in central India was studied, due to its high variability in terrain ruggedness.

A new & comprehensive method of georeferencing LPA image was developed to visualize and measure ICESat footprint over satellite imagery. LPA provides the spatial distribution of the laser energy within footprint. It was georeferenced and converted to KML format to be visualized over Google Earth for better and easy visualization of ICESat footprint.

A code in IDL was developed to simulate ICESat waveform over rugged terrain. CARTOSAT DEM was used as the reference DEM. Simulation results shows very high correlation with ICESat waveforms over flat terrain, with R = 0.987272. In gently sloping agricultural land it was observed that the ICESat full-waveform have recorded the signals from the crop canopy in grown millet or red gram crops. At highly sloping terrain correlation coefficient was R = 0.660186. Geolocation accuracy of the footprint was analysed by simulating waveform after shifting footprint around its original location. Shift of 7.5 m towards south in footprint location, increases the correlation coefficient to R = 0.804606. To analyze the footprint over ravine terrain, input CARTOSAT DEM was enhanced by including field measurements of DGPS. The correlation between simulated waveform and ICESat waveform over ravine terrain after correcting for footprint geolocation, was good with R = 0.851955. It was also observed that when the spatial resolution of the input reference DEM was increased from 2.5 m to 1 m the simulated waveform was in agreement with ICESat full-waveform, with correlation coefficient R = 0.908011. The study highlighted the potentials of ICESat full-waveform over highly rugged ravine terrain.

Acknowledgements

I take this opportunity towards my sincere thanks to Dr. V.K. Dadhwal, Dean, IIRS, for giving me this great opportunity to pursue IIRS-ITC Joint Education M.Sc. Programme 2008-10. I owe my gratitude to him, for all the necessary guidance provided during the course and for all the facilities in IIRS.

Words are inadequate to convey the gratitude to my IIRS supervisor, Mrs. Shefali Agarwal, Head, Photogrammetry & Remote Sensing Division, IIRS. It is my proud privilege to express my deep sense of gratitude to her, for timely advice, support, comments, guidance and encouragement through out my research period. I am also thankful to my second IIRS supervisor, Dr. R. S. Chatterjee, Geo-Science Division, IIRS, for his invaluable suggestion, moral support, and guidance to carry out the field work.

My sincere thanks to my ITC supervisor, Asst. Prof. Dr. Martin Rutzinger, Department of Earth Observation Science, ITC, for his ever enthusiastic spirit, constant support, valuable guidance and critical comments rendered for the improvement, which has contributed to the successful completion of this thesis.

I am extremely grateful to Mr. P.L.N. Raju, In-charge, Geo-Informatics Division for his moral support, encouragement, timely suggestions and guidance for improvement during the research work. I am also thankful to Dr. Sameer Saran, Programme coordinator, M.Sc. Geo-informatics, at IIRS, and Dr. Nicholas Hamm, Programme coordinator, IIRS-ITC JEP, M.Sc. Geo-informatics, at ITC, for his motivation, support and guidance throughout period of research. I am very thankful to all the faculty members of the IIRS and ITC who shared their knowledge with me during the course. My special thanks to IIRS & ITC library that provided me the necessary study material swiftly, whenever required. I am also thankful to the IIRS & ITC staff members who provided their services when ever needed.

I owe my heartfelt gratitude to my Parents Mrs Vimla & Mr. R.D.Yadav, my sister Mrs. Manjula, my brother Mr. Manish & my best friend Shailja, for their support and affection. My sincere thanks to my friends Dipannita, Santosh, Y.K. Laad & all batch mates at IIRS, for sparing their valuable time and resources with me.

Last but not the least; I would like to thank all the members of the Thesis Assessment Board, for critically analysing this thesis.

Table of contents

List of figures

List of tables

1. Introduction

1.1. Full-waveform Laser Altimetry

Laser altimetry is one of the useful remote sensing techniques to measure elevation and monitor changes in the earth surface. A laser altimeter transmits a laser pulse towards the target and records the time-of-flight of a laser pulse to the target and back. This provides the range between sensor and target. Combining range with sensor location and laser pointing angles at the time of each laser shot, will give footprint location on ground.

Earlier laser altimeter systems recorded only single return from each transmitted laser pulse. This gives information about top surface intercepted by laser energy pulse. Then more advanced systems arrived, they are capable of recording multiple returns from single transmitted pulse. This gives information about various levels of elevation within each footprint. Laser altimetry systems are available which can record up to six returns per pulse. Later on new type of laser altimeter systems came into picture, which records and digitizes the backscattered laser pulse into very narrow time intervals, called full-waveform laser altimetry system. It records the backscattered laser energy from various elevation levels on ground as the transmitted laser pulse intersects it with time. Hence full-waveform represents the vertical distribution of the ground surface. Full-waveform is not a continuous representation of vertical distribution of the ground surfaces; rather it represents equally spaced samples, recorded at various elevation levels within footprint (Hofton et al., 2000).

Ice, Cloud and land Elevation Satellite (ICESat) was launched by NASA in January 2003. It is the first and only available space-borne full-waveform laser altimetry satellite. The principal objectives of the ICESat mission were to measure and monitor polar ice-sheet elevation changes; land topographic profile; atmospheric profile of cloud and aerosol properties; height and vertical structure of vegetation canopies (Zwally et al., 2002). Geoscience Laser Altimetry System (GLAS) on-board ICESat transmits the laser pulse of approximately 5 ns width in 1064 nm wavelength for surface altimetry with 40 Hz pulse rate. It records backscattered laser energy from approximately 70 m footprint, with along track spacing of 172 m on ground. In GLAS spatial distribution of the transmitted laser energy within footprint for each pulse is recorded as the Laser Profiling Array (LPA) (Figure 1). LPA measures far field spatial pattern of laser beam energy. LPA is 20 X 20 pixel array imager which operates at 40Hz

to image every transmitted laser pulse (Sirota et al., 2005). The measured beam pattern have a nominal elliptical Gaussian shape, maximum at centre and radial decrease in laser energy for majority of GLAS footprint. The ellipse size of footprints changes in different ICESat laser campaigns. The footprints are more elliptical in earlier campaigns and less elliptical in the later ICESat campaigns. Average major axis of the footprints and average eccentricity for different ICESat laser campaigns are given in Appendix A. Received laser energy from footprint is digitized in 544 bins of 1 ns time interval each. Hence it samples the ground every 15 cm vertical distance and generates full-waveform data (Figure 2). Full-waveform laser altimetry data not only provides the accurate range measurements but also describes the physical and geometrical properties of the illuminated surface or objects as well (Mallet & Bretar et al., 2009).

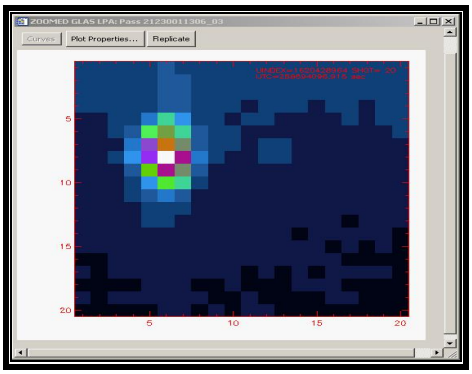

Figure 1 : LPA image of laser shot viewed in ICESat Visualizer Tool.

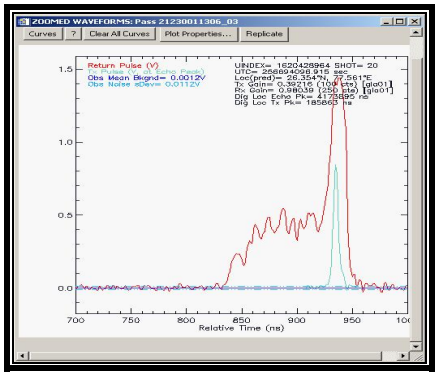

Figure 2 : Full-waveform viewed in ICESat Visualizer Tool.

1.1.1. Physical Principals of Lase r Altimetry

In laser altimetry systems pulsed or continuous laser beam is used to measure range between the sensor and the earth surface. Pulsed system transmits short pulses of the laser towards the target. These pulses are time tagged so that it can be identified separately at recording time. Transmitted laser pulses travel with known velocity in a given medium. Hence by knowing the time delay created by travelling of laser beam from source to the target surface and back to the sensor, distance between sensor and target surface or range can be calculated by Eq. 1 (Vosselman & Mass, 2009). This technique is called time-of flight range measurement.

$$range \quad \rho = \frac{c}{n}\frac{\tau}{2} \qquad \text{(Eq. 1)}$$

τ = round trip time delay of laser beam
c = velocity of light
n = correction factor equal to the reflective index of atmosphere.

Laser altimetry systems determine the 3-dimentional co-ordinates of the point which is intercepted by the laser beam. To calculate the co-ordinates of the footprint on the reference ellipsoid, input information like range measurement, laser pointing vector, sensor position & orientation parameters are required. In the space-borne sensor (GLAS), range distance from sensor to target and laser beam vector information is calculated by Laser sensor unit. The position and orientation of the sensor platform are calculated by GPS and Stellar Reference System (SRS) using Precision Orbit Determination (Rim & Schutz., 2002) and Precision Attitude Determination (Bae & Schutz., 2002) algorithms.

1.1.2. Full-waveform Digitization

Traditional laser altimetry systems can sense only one backscattered echo from each transmitted pulse, which are capable of determining only one point on the ground, from one transmitted laser pulse. This is sufficient if the transmitted laser pulse intersects only one object in its path for example building roof tops, barren terrain etc. But there may be a case when single laser pulse encounters more then one objects within its path for example, a tree. In this case single echo recording systems will record only one point i.e. on the top of the tree, which is not sufficient. New type of LiDAR systems have been developed to overcome this, which are capable to record more then one echo from single transmitted pulse. These systems are known as Multi-echo or Multi-pulse systems. Some systems are capable of recording up to six distinct returns from one transmitted laser pulse (Theil & Wehr, 2004). Multi-echo technique provides returns not only on the canopy surface but also within the tree canopy and ground as well, which is useful to understand the canopy structure and determining the tree height.

A new generation of laser altimetry systems have emerged as advancement in multi-echo technique. These systems are called full-waveform laser altimeter system. Full-waveform systems are capable to record and digitize the whole backscattered laser energy in very small time bins generally 1ns, and full-waveform curve is generated which shows the changes in recorded laser energy with time. Modes in this curve represent the reflecting objects at various elevations. Full-waveform provides additional information about the geometric structure and physical properties of the illuminated objects. It also provides the vertical distribution of the objects within the illuminated surface of footprint.

1.1.3. Full-waveform laser altimetry systems

The first topographical full-waveform laser altimeter system was designed in mid 1990s. They are the experimental systems to study utility of full-waveform for

various objectives i.e. for vegetation structure, DEM etc. The main technological difference between systems are in footprint size, pulse energy and pulse repetition frequency (PRF). Some systems are small footprint and others are large footprint, both systems differ in information type and contents (Mallet & Bretar, 2009).

1.1.3.1. Small footprint Topographic Full-waveform Laser Altimeters

Laser altimetry systems which have footprint in range 0.2 m to 3 m diameter are known as small footprint systems. These systems are air-borne systems. Footprint size depends upon flying height and laser beam divergence. Due to the small footprint size these systems often miss the tree tops, and in dense vegetation it is not sure that laser beam reached up to ground or not (Dubayah & Blair, 2000). Some examples of small footprint laser altimetry systems are ALTM 3100, ALS 60, Mark II, LMS Q560 etc. technical specifications of these systems are given in Table 1.

Table 1 : Small footprint Full-waveform systems

System properties	Small footprint Full-waveform Systems				
	ALTM 3100	ALS60	Mark II	Falcon III	LMS Q560
Company	Optech	Leica	TopEye	TopoSys	Riegl
Platform	Airborne	Airborne	Airborne	Airborne	Airborne
Beginning – Final Year	2004 -	2006 -	2004 -	2005 -	2004 -
Wavelength (nm)	1064	1064	1064	1560	1550
Flying Height (km)	≤ 3.5	0.2 – 6	< 1	< 2.5	< 1.5
Pulse Rate (kHz)	≤ 70	≤ 50	≤ 50	50 – 125	≤ 100
Pulse energy (mJ)	< 0.2	< 0.2	-	-	0.008
Pulse width (ns)	8	5	4	5	4
Footprint size (m)	0.3/0.8 @1km	0.22@1 km	1@1 km	0.7@1 km	0.5@1 km

1.1.3.2. Large footprint Topographic Full-waveform Laser Altimeters

Large footprint systems have footprint diameter from 10 m to 70 m. These systems are mostly space-borne, but air-borne systems are also available which

operates in higher flying height. Due to high flying height, large footprint systems have low pulse firing rate and higher energy laser beam. Because of large footprint size it is more probable that laser beam hit to the canopy top and reached to the underlying ground surface as well. Hence these systems provide signals from the canopy top and ground, both in single transmitted pulse. Large footprint systems are more useful for vegetation studies than small footprint systems. NASA developed several large footprint full-waveform systems to study forest, ocean, cloud, and land topography. Technical specifications of these systems are given in Table 2.

Table 2 : Large footprint Full-waveform systems

System properties	Large footprint Full-waveform Systems				
	GLAS	LVIS	SLICER	SLA-02	ICESat-II
Company	NASA	NASA	NASA	NASA	NASA
Platform	Satellite (ICESat)	Airborne	Airborne	Satellite	Satellite
Beginning – Final Year	2003 -	1997 -	1994 - 1997	1996 - 1997	Planned to be launched in 2015
Wavelength (nm)	1064/532	1064	1064	1064	1064
Flying Height (km)	600	< 10	< 8	285	600
Pulse Rate (kHz)	0.04	0.1 – 0.5	0.075	0.01	0.05
Pulse energy (mJ)	75/35	5	-	40	50
Pulse width (ns)	6	10	4	8	-
Footprint size (m)	66 @600 km	40 @5 km	10 @5 km	85 @285 km	50-70@600 km

Scanning LiDAR Imager of Canopies by Echo Recovery (SLICER), this is the air-borne system designed to study vegetation canopy structure and other vegetation parameters. Similarly Laser Vegetation Imaging Sensor (LVIS), is advancement in SLICER, it is also air-borne full-waveform digitizing laser altimetry system. It is used to measure the vegetation canopy and the ground surface below the canopy as well (Blair et. al., 1999).

Shuttle Laser Altimeter (SLA), was the satellite sensor it was built to take global observations of Oceans, Clouds and Land. Similarly Multi-Beam Laser Altimeter (MBLA) was also space-borne LiDAR remote sensing system. It consist five beams instrument to study environmental issues and carbon stock estimations. It has footprint size of 25m diameter. This program was due to be launched on 2003 but was abandoned.

1.1.4. Geoscience Laser Altimeter System (GLAS)

GLAS onboard ICESat is the only available space-borne laser altimeter system. GLAS was developed by NASA with the primary objective of studying polar ice-sheet using 1064 nm laser, and cloud & aerosol by 532 nm laser (Geophysical research Letters, 2005; NSIDC, 2009). GLAS instrument uses an Nd:YAG laser. It determines the range from round-trip pulse time of the infrared pulse. GLAS instrument is nadir viewing, at altitude of 600km. Footprint diameter on ground is 70 ± 10 m. Pulse frequency is 40 Hz, hence the footprint are separated 172 m apart along track, on the ground (Brenner et al., 2003).

ICESat was planned to be placed in a 183 day ground repeat cycle which will yield 15km spacing between repeat tracks at equator and 2.5km spacing at 80° latitude (Brenner et al., 2003). It could not happen as planned due to the failure of one laser. There are three lasers on GLAS, named Laser-1, Laser-2, & Laser-3. Laser-1 started firing on February 20, 2003 and failed after 38 days of operation on March 29, 2003. Because of the failure of one laser, other two lasers lifetime was reduced. To get the data for longer period of time ICESat mission was re-planned. Temporal repetivity was changed to 91 days repeat cycle with 33 days sub-cycles. Instead of original temporally continuous measurements, the laser was operated for three 33 days sub-cycles per year. Due to this, GLAS measurement duty cycle was reduced from 100% to 27% per year (Abshire et. al., 2005). Three 33 days sub-cycle data have been acquired in Feb-March, May-June and October-November each year. The sub-cycles are named as a, b, c,…..so on, for 33 days campaigns. Laser-2 operated for campaigns Oct-Nov, 2003 (L2a), Feb-March (L2b) and May-June (L2c) in 2004. Use of Laser-3 was initiated in October, 2004 (L3a); and continued in Feb-March (L3b), May-June (L3c), Oct-Nov (L3d) in 2005; Feb-March (L3e), May-June (L3f), Oct-Nov (L3g) in 2006; March-April (L3h), Oct-Nov (L3i) in 2007; Feb-March (L3j), in 2008. During campaign L3k on October 10, 2008 Laser-3 failed. Laser-2 again started in Nov-Dec (L2d) in 2008; and continued in March-April (L2e); Sep-Oct (L2f) in 2009 (NSIDC, 2009). More detailed information about the ICESat campaigns is given in Appendix A.

Digitizer in GLAS temporarily records the signals from entire time-of-flight, the range of around 765km from the surface to the sensor. This generates huge amount of data around 5 million digitized samples of 1ns time interval and 15cm range

resolution sensor can not transmit this huge amount of data. Hence it filters this data using onboard algorithm and extract only transmitted pulse and ground return signals. Recognition of ground return signal is done by using onboard 1 km resolution Global-DEM derived from combination of Shuttle Radar Topographic Mission (SRTM) & Global 30 Arc-second elevation dataset (GTOPO30). Surface finding algorithm in GLAS extracts 544 sequential samples and transmits it to the ground (Zwally et. al., 2002).

Sirota et al., (2005), described the method of laser pointing and attitude determination of GLAS. This was accomplished through Precision Attitude Determination (PAD) algorithm onboard GLAS. PAD uses data gathered from Stellar Reference System (SRS) onboard GLAS. SRS consist of Laser Reference Sensor (LRS), Attitude Determination System (ADS), and Laser Profiling Array (LPA). ADS measures the orientation of the instrument platform with respect to the star field and the LRS is a narrow FOV camera operating at 10Hz frame rate. ADS and LRS are aligned to determine the attitude and orientation of the instrument with respect to stars. Another component of SRS is Laser Profiling Array (LPA), it is an 80 X 80 pixel array image. LPA has same IFOV as LRS and operates at 40Hz. Thus LPA images every transmitted laser pulse. Although LPA is 80 X 80 pixels image, but only the 20 X 20 pixel image containing the footprint illuminated area, is transmitted to the ground. LPA is 8-bit image of transmitted laser beam. It shows the spatial distribution of the laser energy within footprint.

1.1.5. Full-waveform Modelling Techniques

Earliest work to model backscattered full-waveform was done by Gardner, (1992), he described the theoretical model for full-waveform satellite laser altimeters over simple, un-vegetated surface. Abshire et al. (1994) described the characteristics of backscattered full-waveform for simple one-dimensional surfaces. Blair & Hofton (1999) modelled the laser altimeter return full-waveform as the sum of reflections within footprint. They assumed that the waveform shape represents the vertical distribution of within footprint objects. Waveform shape also account for spatial distribution of laser beam intensity along and across the beam path and impulse response of altimeter receiver. For vertical distribution of within footprint surface they used regularly spaced elevation data. They assumed the same reflectivity within footprint. In their model, backscattered full-waveform is composed of sum of elementary pulses reflected from each object within the footprint. Sum of elementary pulse is convolved with the Gaussian function. They have generated model waveform (y) using Eq. 2 (Blair & Hofton, 1999).

$$y = I(z) * \sum_{i=1}^{m} \sum_{j=1}^{n} e^{-d_j^2 / 2\sigma_f^2} \; e^{-(z-h_j)^2 / 2\sigma_p^2} \qquad \text{(Eq. 2)}$$

Two Gaussian functions represent the spatial distribution of laser beam intensity across and along beam path respectively.

Harding & Carabajal (2005) described the full-waveform modelling for GLAS waveform. They expanded the approach of Blair & Hofton. For the laser beam intensity distribution across and along beam path, they used LPA images and GLAS transmitted pulse waveform. An LPA image of the transmitted pulse is used for spatial distribution of laser energy within footprint and GLAS transmitted pulse waveform is used for temporal or along beam path distribution of laser energy. Thus instead of two Gaussian functions used in the Eq. 2 by Blair & Hofton, they used two parameters LPA and GLAS transmitted waveform. They used high resolution DEM prepared by airborne lidar. By simulation the GLAS full-waveform they evaluated the geolocation accuracy of the GLAS footprints. They have generated the simulated waveform around the footprint geolocation given in the ICESat data. They computed the full-waveform around the footprint by shifting the LPA over DEM with 9.1 m increment. The computed waveform was then matched with the ICESat waveform, and the best match was identified as the location where the correlation coefficient was maximized.

Sun & Ranson (2000) included laser pulse across and along beam intensity distribution by dividing vegetation canopy into 3D cells. Cell thickness was equal to the vertical resolution of the sensor, to correspond temporal or along beam distribution of the laser energy. For across beam distribution of laser energy, weight is assigned to the 3D cells such that they represent the Gaussian distribution. More in the centre of the footprint and reduces towards the margins. Weights are 1.0 in the centre cells and reduced by e^{-2} towards the margin of footprint. The waveform was calculated by summing the volume of canopy cells at same height from ground.

Yong et al., (2006) modelled the ICESat full-waveform for forest canopies and described the effect of the terrain slope in forest parameter estimation from full-waveform. Instead of assuming the same reflectance from various objects within the footprint, they included the vegetation crown scattering coefficient, transmittance coefficient and ground reflectance for 1064nm wavelength laser.

Duncanson et al., (2009) described the method to simulate the ICESat full-waveform for estimation of forest canopy height and high relief terrain. They used air-borne LiDAR data as reference data for full-waveform simulation. They analysed the effect of terrain relief on the GLAS waveform to model forest height.

1.2. Rugged Topography

Ravine topography is highly rugged topography. A ravine is a very small valley, almost like a narrow canyon, which is often a product of surface runoff erosion. Surface runoff generates small streams which flow along the slope towards the river or large stream, this drainage generates a very complex stream network, which continuously erode the soil and makes deep gullies, after a long period of erosion deep ravines are formed. Ravines are classified as larger in scale than gullies, although smaller than valleys. Ravine is generally sloping landforms of relatively steep sides. Ravine is an intricate system of deep gullies, running more or less parallel to each other and meeting a nearby river or a regular stream, flowing much lower than the surrounding land (Sharma 1979).

Figure 3 : Ravine Topography at Chambal.

1.3. Problem Definition

ICESat was developed primarily to measure and monitor polar ice-sheet, but researchers have used ICESat full-waveform laser altimetry data to extract vegetation parameters like canopy height, canopy vertical structure, crown depth, outer canopy ruggedness and a measure of canopy cover (Anderson et al., 2006; Drake et al., 2002; Hyde et al., 2005; Sun et al., 2008). In areas where topographic relief within laser footprint is small compared to tree heights, the waveform typically shows distinct modes in the curve (Figure 4). One mode represents the ground return and other represents the return from vegetation canopy. Analysis of this kind of waveform will provide estimation of various bio-physical parameters. On the other hand such areas where within footprint topographic relief is a substantial fraction of tree height, the canopy and ground returns are mixed together (Harding et. al., 2005). Waveform dose not have distinct modes in curve, rather these curves are intermixed (Figure 5). Hence the resultant waveform over the rugged topography becomes complex. It is difficult to estimate bio-physical parameters from laser full-waveform over rugged terrain.

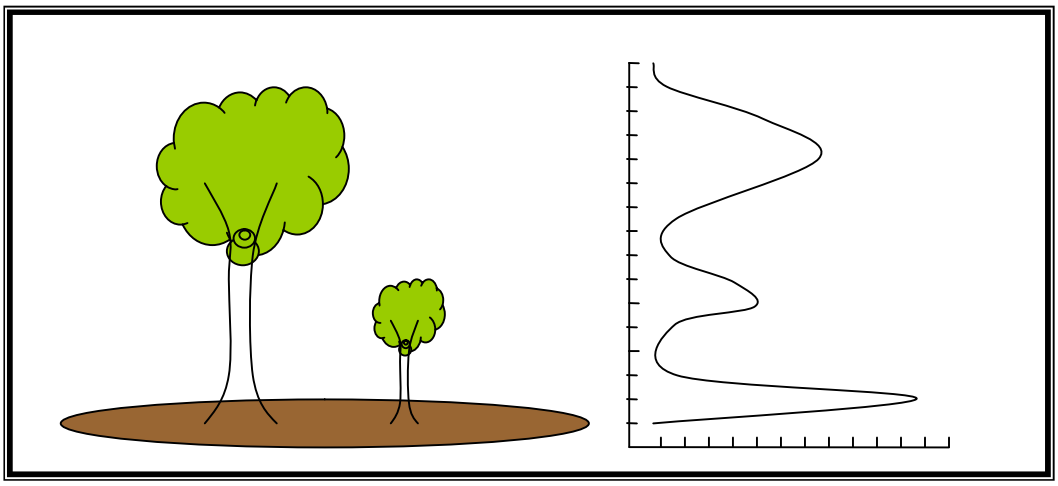

Figure 4 : Full-waveform over flat terrain with distinct modes for canopy and terrain

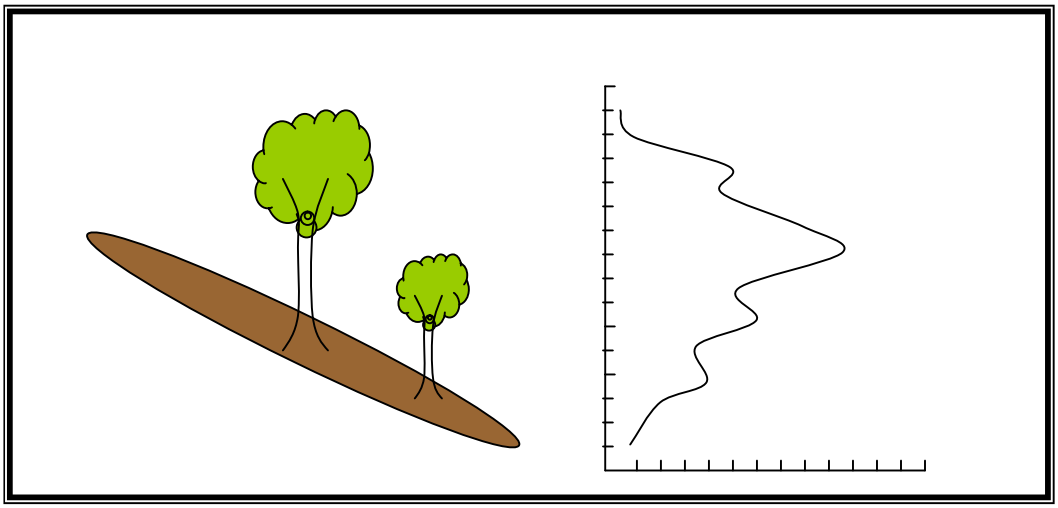

Figure 5 : Full-waveform over rugged terrain with mixed signals from canopy and terrain

1.4. Research Objective

The objective of this research work is to understand the characteristics and behaviour of the ICESat full-waveform data over highly rugged topography. This will be achieved by simulating the ICESat full-waveform over highly rugged Ravine terrain. Chambal Ravines in the central India is studied for that purpose.

1.5. Research Questions?

1. What parameters will be required to simulate the ICESat full-waveform over highly rugged terrain?

2. How to georeference the LPA images to get better visualization of the ICESat footprints over terrain?
3. How well the actual ICESat full-waveform can be represented by simulated waveform over different terrains?
4. How the ICESat full-waveform behaves over different terrain?

1.6. Research approach

To fulfil the objectives of the research, GLAS data was analysed over terrains with different ruggedness by simulating the GLAS full-waveform. Highly rugged ravine area of Lower Chambal valley in central India was selected for the study. The GLAS data lying within the study area was downloaded and pre-processed. An algorithm was developed in IDL to generate the simulated full-waveform. Field work was carried out to collect within footprint ground truth data (ravine depth, terrain slope, land cover categories). Differential-GPS measurements were taken within footprint to refine the DEM and to validate the simulated waveform. The results of the algorithm were compared with the ICESat recorded waveform. Geolocation accuracy of the ICESat footprints was evaluated by simulation of full-waveform after shifting the footprint geolocation to different directions around the original location. The footprint shift, with highest correlation provided more accurate geolocation of the footprint.

2. Study Area

2.1. Selection of the Study area

To fulfil the research objective, a highly rugged terrain was considered that had the variability in terms of terrain ruggedness. For the study three terrain types viz. high sloping terrain, very rugged terrain and flat terrain was selected. Another requirement was the availability of the ICESat footprints over such terrain features. And the footprint should be accessible on ground. Therefore part of Lower Chambal Valley in the central India was selected for study in this work. Study area has the ICESat track running across the ravine area, high sloping area and flat agricultural fields (Figure 7a, 7b, 7c & 8). The area has enough terrain variability and ICESat footprints were also available and accessible as well.

2.2. Location

A highly rugged ravine area was selected for this study. This area belongs to a part of Lower Chambal Valley in central India. Area lies in the southern part of Karauli District in Eastern Rajasthan, India. In the Lower Chambal Valley ravine topography has been developed in both sides of the Chambal River. Area in north part of the Chambal River, near town Mandrayel in Rajasthan was selected due to availability of the ICESat data and its topographical characteristics. The GLAS footprints were available west of the small town Mandrayel, near village Khirkan, and Mungepura in Karauli District of Rajasthan (Figure 6).

2.3. Geomorphology of Chambal Ravine

Studies of Sharma (1979) described that geologically, Lower Chambal river valley is geotectonic zone formed mainly by the Vindhyan sediments lying on the Archean foundation. A major portion of the valley is covered by recent and sub-recent unconsolidated sediments. In this portion very intense ravines are still developing. The location of the region itself is significant the lower Chambal valley lies at the junction between the South-eastern fringe of Aravalies and north-western lobe of the Great Vindhyan plateau of central India.

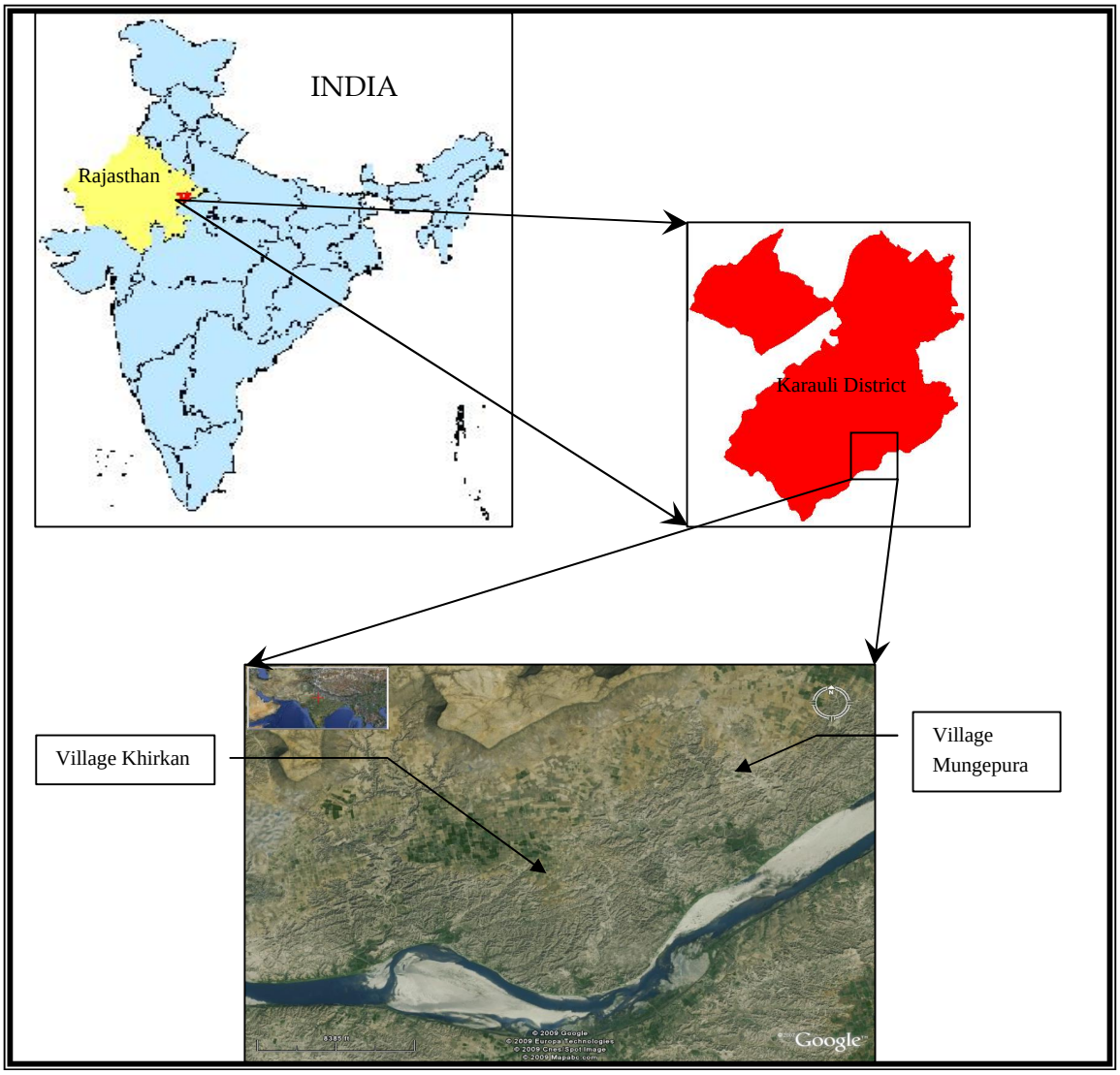

Figure 6 : Location of Study Area (courtesy: Google Earth)

The great boundary fault of Rajasthan runs along the valley and roughly bifurcate valley into two parts. The North-western part comprises intensely folded Archean formations while South-eastern part is composed of horizontally reposing Vindhyan systems.

Soil characteristics, upliftment of land and ecological factors have played an important roll in the formation of ravines in Chambal area. Ravine erosion is a function of soil type, geology, and slope, character of stream, rainfall and upliftment. Studies about the genesis of the ravines in Chambal area, shows that the Chambal River and its tributaries were rejuvenated due to the tectonic activities in Pleistocene and Recent times (Chatterjee et al., 2009; Sharma, 1979). Due to the tectonic activities the elevation difference between Chambal River bed and its surrounding area, was increased. This causes rapid erosion on the Chambal River bank by its tributaries and streams. Soft

alluvium and sandstone present in the area supported the erosion and dense ravine topography was developed.

2.4. Terrain characteristics of the study area

In the study area according to the ruggedness, terrain can be roughly classified into three parts (Figure 8). In the northern part of the study area there is a large sloping terrain of approximately 150 m of length (Figure 7A). This is followed by flat agricultural field (Figure 7B) and in the southern part of the study area dense ravines are present (Figure 7C) in approximately 2 km wide band in the northern bank of Chambal River.

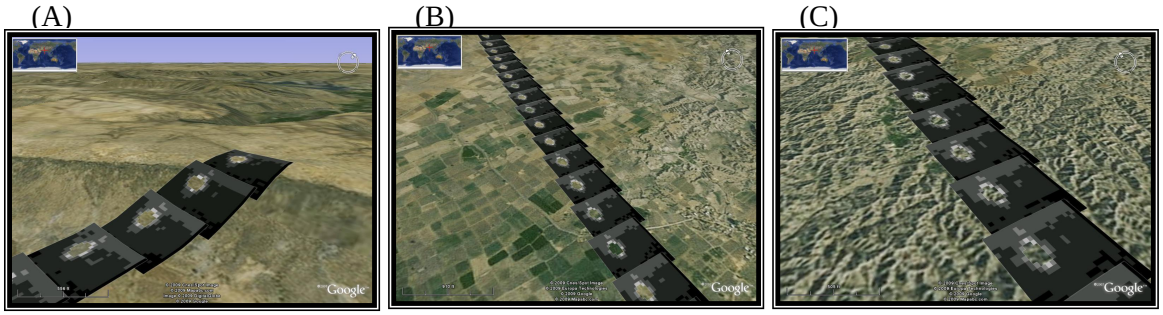

Figure 7 : GLAS footprints over different terrains in the study area. (A) Footprint over highly sloping terrain, (B) Footprints over agricultural fields, (c) footprints over ravines. (courtesy : Google Earth).

The sloping terrain is dipping towards the south direction. The slope is large and concave. In the top portion it is very steep and decreases gradually downwards (Figure 7A). GLAS footprint is present in the middle part of the slope where the amount of slope is between 45° – 65°.

The ravines present in the study area are very intense and field observations using the Laser Distance Meter and Differential-GPS shows that the average depth is between 15 – 25 m. Density of ravine is high. The sides of the ravines are very steep, the top portion is highly steep with 60°-75° slope, the intermediate part have slope between 40°-60° and the bottom level have slope from 15°-25°. Ravines are U-shaped with nearly flat bottom.

2.5. Landuse & Landcover in the study area

The Chambal region is mainly a rural area. The soil in the area is sandy-clay soil. Thick layer of alluvium is present in the area, which is unconsolidated. Hence it

eroded easily and swiftly which supported the formation and development of ravines in this region.

The climate is semi arid with very high temperature variation and an irregularly distributed rainfall. The vegetation cover is very less. Thorny shrubs are present in the area. The Northern part of the study area is covered with the shrubs and fragmented rocks. In the middle part of the study area agricultural fields are present. In the study area, mainly two crops are present i.e. Red Gram & Millet. The cultivation depends upon the monsoon. The Red-Gram is usually cultivated in period from July to March and Millet is grown in the fields in period from July to October.

3. Materials & Data sets used

3.1. GLAS Data

Full-waveform laser altimetry data of ICESat was used in this research. ICESat data from orbit reference ID 2123 was analysed. Data was acquired during the Laser L3j campaign on 17th March 2008. This orbit is transacting the study area from north to south and passing over different type of terrain (Figure 8).

Figure 8 : Google Earth image of the study area and the ICESat orbit 2123 (Red line). (courtsey : Google Earth)

ICESat provides 15 standard data products (GLA01 to GLA15). Each product is developed and processed for specific uses. Table 3 provides specifications of different data products of ICESat. The data is processed to different levels viz. level-0 to level-3. Level-0 is a raw telemetry data, level-1 data products includes instrument parameters, level-2 data products have geophysical, ice, ocean, atmosphere and land parameters. Level-3 products provide gridded digital elevation model and atmospheric backscattered images. Data is distributed by National Snow and Ice Data Centre

(NSIDC). All data products are time-stamped, with transmit time of pulse in Coordinated Universal Time (UTC), as collected along track. Data products are distributed in granules, which contains different amount of data. All data products have different structure, variables and size of data. To correlate records across GLA01 – GLA15 a unique record index is assigned to every one second of data. The unique record index is consistent across all products of the same release. Small changes may exist between different data release. For example record index scale factor is changed from 10 to 5 in latest data Release-31 available from December, 2009. GLAS data products are provided in single integer binary format.

Table 3 : ICESat/GLAS Standard Data Products (NSIDC).

Short Name	Long Name	File Size	Orbits per File
GLA01	L1A Global Altimetry Data	9 MB	1/4
GLA02	L1A Global Atmosphere Data	671 MB	2
GLA03	L1A Global Engineering Data	19 MB	2
GLA04	L1A Global Laser Pointing Data	2 MB - 386 MB	2
GLA05	L1B Global Waveform-based Range Corrections Data	25 MB	1/4
GLA06	L1B Global Elevation Data	7 MB	1/4
GLA07	L1B Global Backscatter Data	827 MB	2
GLA08	L2 Global Planetary Boundary Layer and Elevated Aerosol Layer Heights	7 MB	14
GLA09	L2 Global Cloud Heights for Multi-layer Clouds	82 MB	14
GLA10	L2 Global Aerosol Vertical Structure Data	289 MB	14
GLA11	L2 Global Thin Cloud/Aerosol Optical Depths Data	13 MB	14
GLA12	L2 Antarctic and Greenland Ice Sheet Altimetry Data	104 MB	14
GLA13	L2 Sea Ice Altimetry Data	107 MB	14
GLA14	L2 Global Land Surface Altimetry Data	209 MB	14
GLA15	L2 Ocean Altimetry Data	279 MB	14

For the study following three data products of GLAS are used

- L1A Global Altimetry data (GLA01),
- L1A Global Stellar Reference and GPS data (GLA04), and
- L2 Global Altimetry data (GLA14).

Global altimetry data (GLA01) is level 1A data. One granule contains 1/4th of the orbit or ~23 minutes of data. This data can be searched by time or granule ID. Spatial search is not available in this data product. The variable list of the GLA01 data product is given in Appendix B. GLA01 contains the transmitted and received echo waveforms.

The transmitted pulse is recorded into product variable named i_tx_wf. The ordering of the transmitted pulse is preserved as the telemetered pulse, so it is in time order. The value of the first sample is for the sample closest to the spacecraft in time, and the value of the last sample is for the sample farthest from the spacecraft in time.

The received echo waveform is recorded into i_rng_wf variable of GLA01. It is preserved as the telemetered echo, so essentially it is in time reversed order. The value of the first sample is for the sample farthest from spacecraft in time, and value of the last sample is for the sample closest to the spacecraft in time.

Global Stellar Reference & GPS data (GLA04) is level 1A data product of GLAS. Its one granule contains 6 hrs. of data, file size is around 610 MB. One data granule of GLA04 contains six separate files, postfixes with no. 1, 2, …, 6. Each file contains different type of information. File 1 of GLA04 was used in this work, which contains the LPA image of the footprint. Granule of GLA04 can only be searched by time or granule ID. Variable list of the GLA04 data product is given in Appendix C. Variable i_PixInt contains the 20 X 20 array of digitized intensity values of cross profile of the laser transmitted beam. The laser energy is digitized in 8 bit. Each shot is given a unique record index number in which 40 LPA images of 1 ns interval are stored.

Global Land Surface Altimetry data (GLA14) is a level 2 data product of GLAS. It contains maximum amount of information about land surface altimetry. One granule of the GLA14 contains 14 orbits of data. GLA14 can be searched either temporally or spatially. Variables contained in GLA14 are listed in Appendix D. Variable i_lat & i_lon contains the Latitude and Longitude of each footprint, in micro degree. These coordinates are calculated by the algorithm given by Schutz et al., (2002). The algorithm calculates footprint coordinates for every laser pulse in International Earth Rotation Service (IERS) Terrestrial Reference Frame (ITRF).

3.2. Tools to read and visualize GLAS data

GLAS data is provided in single integer binary file. Each data product has different file structure and variables. To read and visualize these binary files some tools developed in Interactive Data Language (IDL) are provided in NSIDC website.

GLAS reader tool is a group of IDL functions to read various GLAS data and output all variables into ASCII format. There is separate IDL function for each GLAS data product. It can be run through IDL or IDL Virtual Machine. They are freely downloadable from NSIDC website.

GLAS Visualizer tool is a useful GUI tool to visualize each GLAS data with its attributes. It reads the data from GLAS file and view graphical summary of the variables. Waveform from GLA01, range & footprint coordinates from GLA14 and corresponding LPA image can be visualized simultaneously (Brenner et al., 2008).

GLAS Ellipsoid Conversion tool is an IDL function which converts the footprint coordinates from GLAS ITRF system to WGS-84 system.

3.3. Field Data Collection

Field work was carried out in month of Nov 2009. The aims of the field work were to make measurements of relief variations within the footprint over ravines, measurements of the slope within the footprint terrain and collection of data about the landcover within the footprint. The information was collected over four footprints with different terrain ruggedness and landcover.

Relief variations in the ravine area within footprint were measured using two instruments viz. Differential GPS & Laser distance meter. Leica GPS System 500 was used to receive signals from GPS satellites which are the processed to obtain a position on earth's surface. Main components of the System 500 are the GPS Antenna, GPS receiver and Terminal. GPS antenna AT501 was used; it is the L1 single frequency antenna. GPS receiver processes the GPS signals received by the antenna. Leica GS50 receiver was used; this receiver is specifically designed for GIS applications. Terminal TR500 was used; which provides the user interface for the receiver.

Rapid static measurements were made using two GPS units. One GPS unit was established as the reference base station and other GPS unit was used are the rover unit to make measurements within footprints. Location accuracy in Differential GPS measurements was 2 - 3 meter. Measurements were taken on each level of the ravines within footprint.

Depth of ravines and slope of terrain within footprint was measured using Laser distance meter Leica DISTO. It provides precise distances between objects. The depth was measured by standing in the bottom level of the ravines and pointing the laser to the top of the ravine.

The information about the landcover within the footprint was collected by visual observations and by interacting with farmers. The information about the time & type of cropping and its height was gathered from the farmers.

3.4. Reference DEM

In this work CARTOSAT-1 DEM was used as the reference DEM (Figure 9). The data was of row 0276 and path 0528. The date of pass was 27th September 2006.

CARTOSAT-1 was launched by Indian Space Research Organisation (ISRO) in year 2005. It has ability to provide along track stereo images with its two PAN cameras on board. One looking 26° fore and another is looking -5° aft from nadir. Spatial resolution of the CARTOSAT-1 is 2.5m.

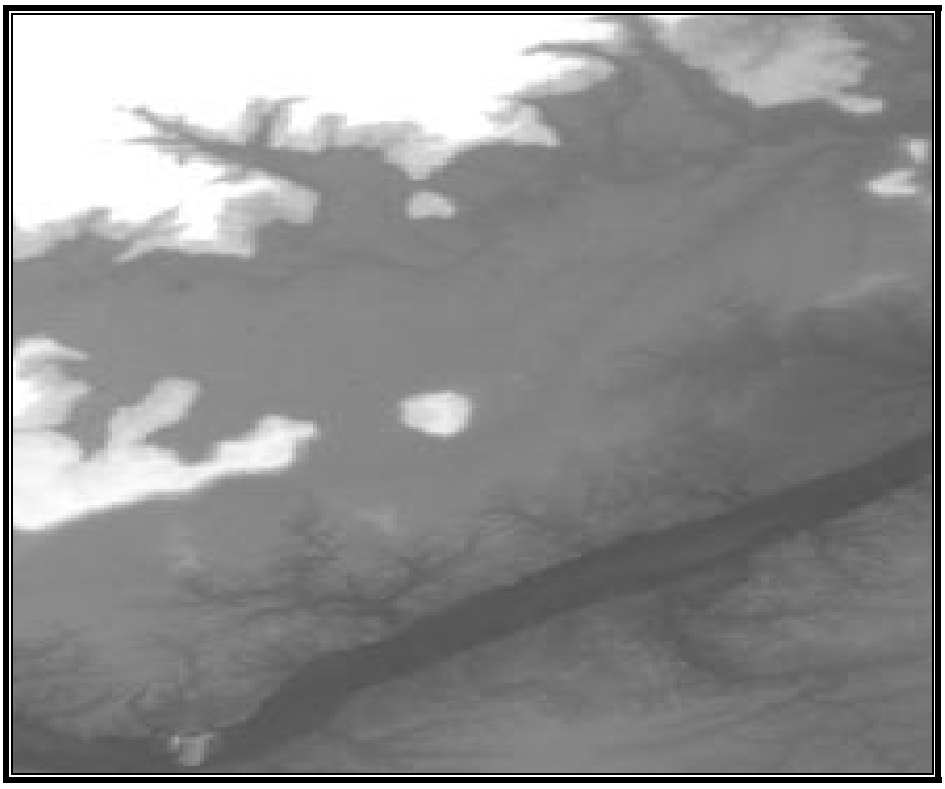

Figure 9 : CARTOSAT-1 DEM of Chambal Ravine Area

4. Methodology

4.1. Full-waveform Simulation algorithm flow-chart

Figure 10, shows the flow chart of the simulation algorithm.

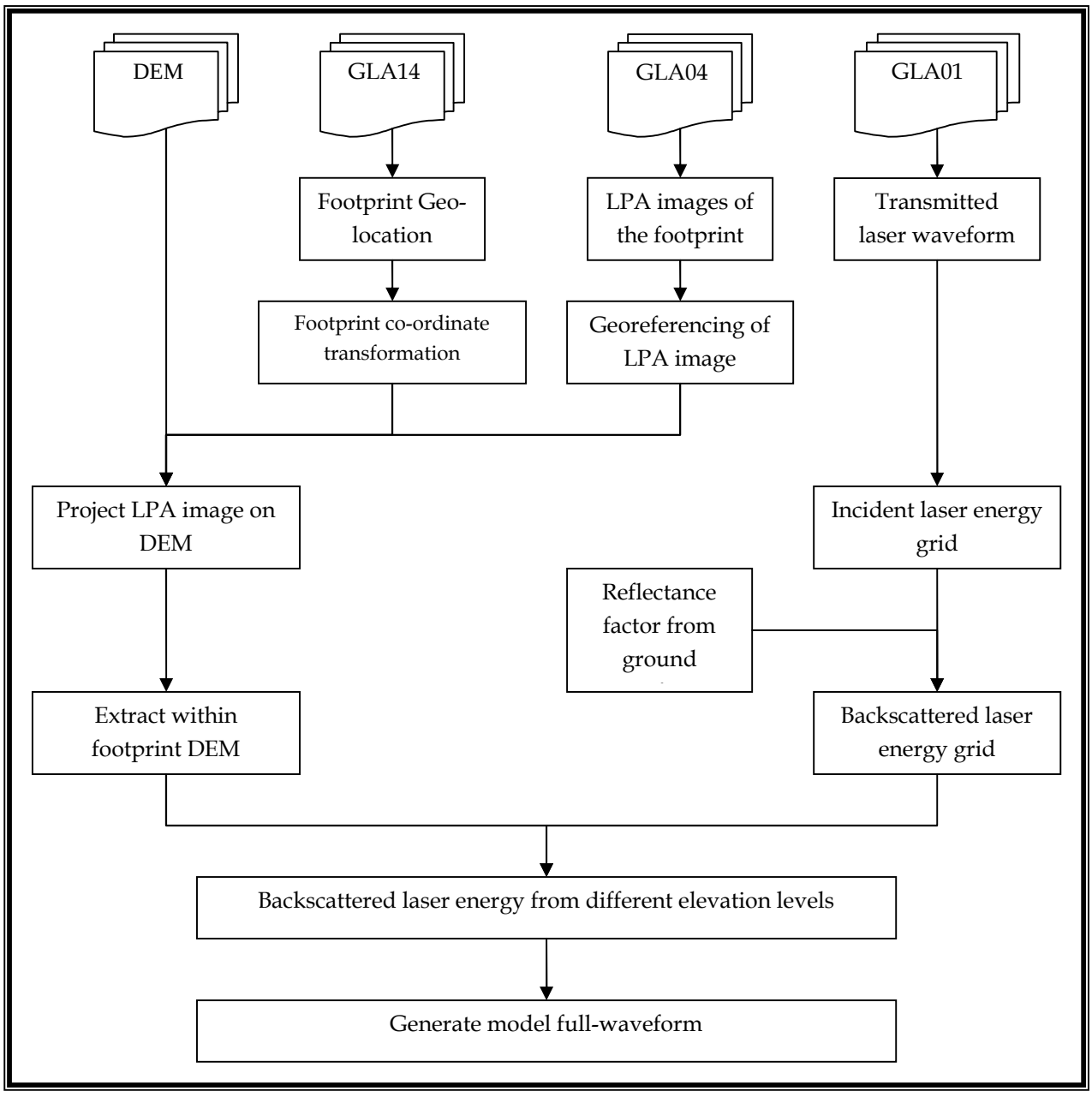

Figure 10 : Flow Chart of the Simulation Algorithm

4.2. Input parameters for full-waveform simulation algorithm

For simulation of ICESat full-waveform three parameters were required. One was reference DEM to represent the terrain. CARTOSAT DEM was used as reference DEM in this work. Second input was the spatial distribution of the laser energy within footprint. LPA images were used for this input. Third was the temporal distribution of the laser energy within single pulse. Transmitted waveform was used for this input, which was given in GLA01 data product.

4.3. Pre-processing & Extraction of data

In this study CARTOSAT DEM was used as reference DEM input. DEM was prepared in 2.5 m pixel size. CARTOSAT DEM over ravines was further refined by adding field measurements from Differential-GPS & laser distance meter. Measurements of Differential-GPS and laser distance meter were taken such as it represented the height variations in the ravines. Measurements were taken in all the levels of the ravines, within footprint. Using these measurements, within footprint DEM was interpolated.

GLAS data within the study area was extracted by first searching for GLA14 data granules, using spatial searching. GLA14 data granule was opened in GLAS Visualizer tool and record index numbers of shots within study area searched from 14 orbits data. These record index numbers were used to extract the required data from the GLA01 and GLA04 data products. Using the GLAS reader tools the data was read and all the variables were printed in ASCII format. Code was developed in IDL to read required variables from ASCII file and place them into IDL variables to further use them in the algorithm.

Footprint coordinates for each shot was extracted from GLA14 data product. These coordinates were in GLAS ITRF coordinate system. These coordinates were transformed into WGS-84 system using the GLAS Ellipsoid Conversion tool.

4.4. Geo-referencing & Visualization of LPA images

LPA image of each laser footprint was extracted from GLA04 data into ASCII format. Then it was imported from ASCII into 20 X 20 pixel raster image. Footprint coordinates and range of corresponding footprint were extracted from GLA14 data product.

To project the LPA image into the geographic coordinate system, its spatial resolution was required. Spatial resolution of each LPA image was calculated using the range given in the GLA14; Field-of-View (FOV) of the LPA image which is 0.08° (Bae &

Schutz., 2002); and number of pixel or dimension of LPA image which is 80 X 80, because the LPA camera captures 80 X 80 pixel image from which only 20 X 20 pixel image is transmitted.

Following formula (Eq. 3) was developed to calculate the spatial resolution of each LPA image separately. The average spatial resolution of LPA images were 10.43 m.

$$r = \frac{2\pi \times \phi \times \rho}{360 \times n} \qquad \text{(Eq. 3)}$$

where r = Spatial resolution of LPA image
ϕ = FOV of the LPA (0.08°)
ρ = Range (in meters)
n = Dimension of LPA image (80 pixels)

The footprint coordinates provided with GLA14 data product was of footprint centre. In LPA image footprint centre is the pixel of maximum energy, because in laser beam, energy is maximum at the centre and it decreases towards the margins (Figure 11).

To geo-reference LPA image, footprint co-ordinates given in GLA14 was assigned to the centre pixel or pixel of maximum value in LPA image and the coordinates of four more points at margin of LPA toward North, East, South & West of the centre pixel were calculated using the Vincenty's direct formula. Coordinates of any point can be calculated From Vincenty's direct formula, by providing the coordinates of known point, and distance & bearing between known & unknown points. To geo-reference LPA image starting point was given as coordinates of the footprint centre; distance between footprint centre and margin point was calculated as number of pixel between two points multiplied by spatial resolution of LPA image; and bearing was given as 0°, 90°, 180°, 270° for North, East, South, West respectively.

After calculating coordinates of points at margin of the LPA towards North, East, South and West of the centre pixel, these points were used as ground control points to geo-reference LPA image in ERDAS Imagine 9.2.

Geo-referenced LPA images were converted to KML file and visualized over Google Earth (Figure 7 & 12). By georeferencing LPA images ICESat footprint can be effectively visualize over Google Earth or any other geo-referenced imagery, footprint shape and size on the ground can be determined. This will also be useful to identify landuse & landcover within the GLAS footprint.

An LPA image has pixel values which represent digitized values of the transmitted laser beam intensity. The digitization is done in 8-bit, hence minimum & maximum range of pixel values are 0 & 255 respectively. In the LPA images used in this study, the pixel values ranges between 67 & 82 (Figure 11).

Figure 11; of the georeferenced LPA image shows that, the Laser energy is concentrated in one elliptical region of the image. This is the region of the footprint. The pixel values in the LPA image was ranging from 67 to 82. LPA image was thresholded by pixel value 70 to represent the energy distribution only within footprint.

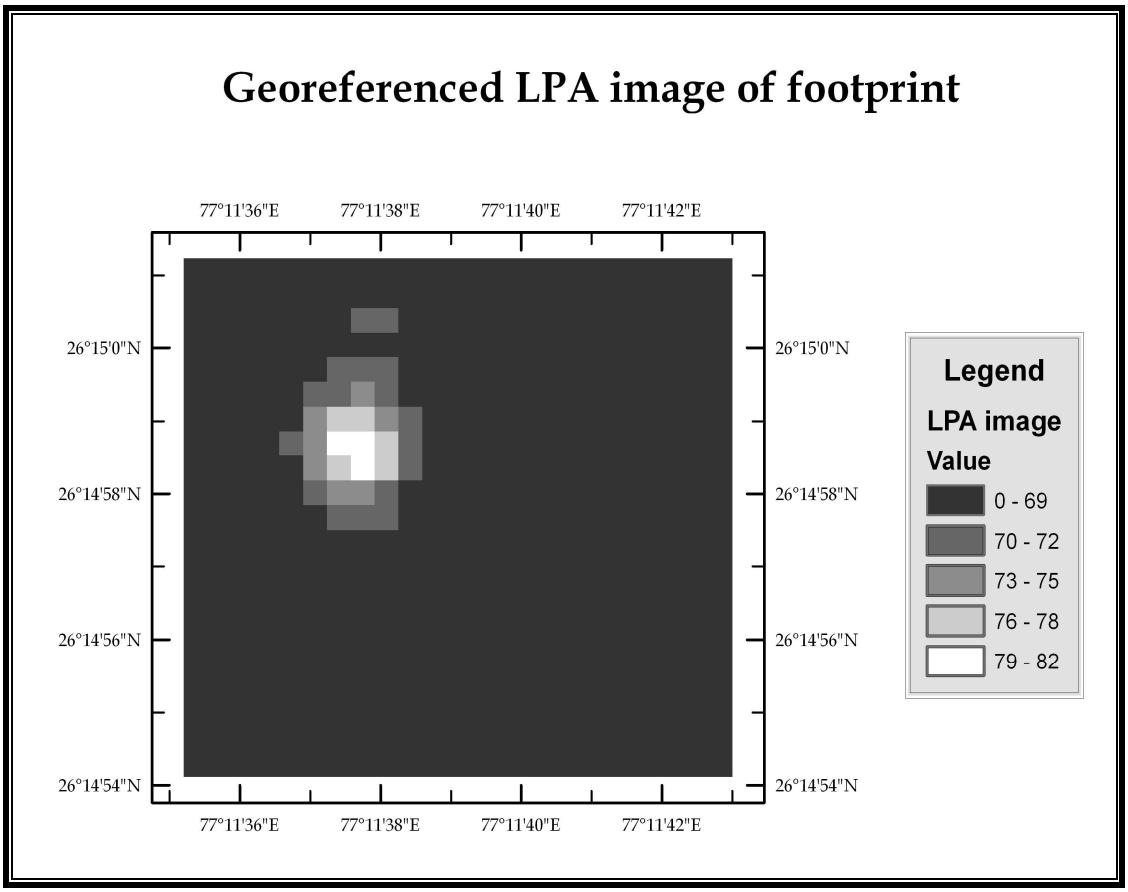

Figure 11 : Georeferenced LPA image of ICESat footprint

4.5. Full-waveform Simulation Method

Full-waveform is a digitization of backscattered laser energy as a function of time. Considering this principal, backscattered energy at each nanosecond interval was calculated and placed into waveform bins. To calculate the backscattered laser energy in each nanosecond, transmitted waveform was convolved with the within footprint DEM.

In this algorithm incident energy on each DEM pixel was calculated. Incident laser energy is a function of laser beam temporal & spatial distribution. Temporal distribution for each nanosecond was extracted from transmitted digitized waveform. And spatial distribution was derived from the LPA image. Spatial & temporal distribution of incident laser energy describes how much laser energy was incident in one nanosecond & how it was distributed spatially within footprint DEM. Hence incident laser energy over each DEM pixel in one nanosecond was derived.

Incident energy was then reduced by reflectance factor. Reflectance factor was roughly estimated by calculating top of atmosphere reflectance from Landsat TM band-4 (750 – 900 nm), which is near to the 1064 nm wavelength laser beam of GLAS.

The terrain surface at the same elevation will backscatter the laser energy at the same time. Hence backscattered laser energy from DEM pixels at same elevation will be combined and recorded into the bin of recorded waveform. ICESat vertical resolution is 15 cm. Hence the DEM pixels within each 15 cm vertical interval was combined and recorded into one bin of the simulated full-waveform.

4.6. Refinement of the DEM using Field Measurements

The CARTOSAT DEM over the ravines area was refined by adding the field measurements of variations in terrain relief. During the field work DGPS measurements at different levels of the ravines were made. Within footprint DEM was interpolated after adding DGPS measured points into it. The resultant interpolated DEM was better representing terrain relief within footprint.

4.7. Footprint Geolocation accuracy

ICESat/GLAS footprint has some geo-location errors due to the misalignment of Field of View (FOV) of the sensor. When within footprint and its surrounding terrain is flat than the footprint geolocation errors do not show much effect in the terrain because the homogeneity in the terrain. However when the terrain is rugged and within footprint relief variations is high then the footprint geolocation error is important parameter. Change in the footprint location will change the vertical distribution of the surface within footprint. This will affect the waveform shape also.

The geo-location error was evaluated by generating the simulated full-waveform after slightly shifting the LPA over the DEM around the footprint location. Then simulated waveform was correlated with the actual full-waveform. The shift in the footprint location for which the correlation was maximum, represented the geo-location error in the ICESat/GLAS footprint.

The LPA image was shifted from the footprint centre location by 5 m (two DEM pixels), 7.5 m (three DEM pixels) & 10 m (four DEM pixels) towards North, East, South, & West. Waveform was simulated again for each shift and correlated with the ICESat recorded waveform.

5. Results & Discussions

5.1. Clasification of the GLAS footprints according to terrain Characteristics

In this study ICESat data of orbit reference ID 2123 was analysed. The ICESat track traverses the study area from North to South and passes over different types of the terrain in the study area. 40 footprints of one second of data from Index No. 1644167754_0 to 1644167754_39 runs across the study area. LPA images of all the 40 footprints were georeferenced and converted to KML format. These georeferenced images were then placed over the Google Earth to visualize the location of the footprint on the ground (Figure 7 & 12). By visual interpretation of the within footprint features, terrains with different ruggedness were identified. On the basis of the terrain ruggedness all the footprints were classified. Classification of footprints is given in Table 4. After visually classify the footprints the verification was done by ground observations. Characteristics like average slope, landuse/landcover and terrain ruggedness of the within footprint terrain was observed on the ground.

Figure 12 : LPA images of GLAS footprints over Google Earth. (courtesy : Google Earth).

Table 4 : Classification of footprints

Footprint ID	Terrain Ruggedness	Landuse/Landcover	Average Slope
1644167754_0	Flat terrain	Barren terrain	< 5°
1644167754_1 to 1644167754_2	High Sloping terrain	Small shrubs are present over slope	45° to 75°
1644167754_3 to 1644167754_18	Gently sloping and flat terrain	Some area is covered by agriculture and some are void of vegetation.	30° to < 5°
1644167754_19 to 1644167754_30	Highly rugged Ravine terrain	Barren land with very less vegetation.	15° to 30°.
1644167754_31 to 1644167754_34	Horizontal & smooth	Above river water	0°
1644167754_35 to 1644167754_39	Gently sloping	Agricultural fields	< 5°

5.2. Results of the Simulation Algorithm

An algorithm was developed to simulate ICESat full-waveform. This algorithm was tested over four different types of terrains i.e. flat terrain, gently sloping agricultural fields, high sloping terrain and highly rugged ravine topography. All four types of terrains have different characteristics and geometry. The full-waveforms over these terrains were simulated using the developed algorithm. These simulated waveforms were then correlated with the ICESat waveforms to validate and optimize the simulation results.

5.2.1. Simulation results over Flat Terrain without vegetation

5.2.1.1. Within footprint terrain characteristics

Footprint 1644167754_10 was analysed which lies over flat terrain. The terrain is barren and void of dense vegetation, only small vegetation like small grass or shrubs are present. The relief variations in the terrain are very less. The standard deviation of the heights within footprint is 0.482176.

5.2.1.2. Simulated waveform

The ICESat full-waveform over flat terrain is shown in Figure 13 with thick black curve. It is narrow and showing Gaussian nature, because of the flat reflecting surface.

Simulated waveform for the flat terrain is also Gaussian in nature and showed very high correlation with the ICESat waveform (Figure 13). Pearson's correlation coefficient between ICESat waveform and simulated waveform was 0.987272, which is very high. Simulated waveform was generated using the CARTOSAT DEM.

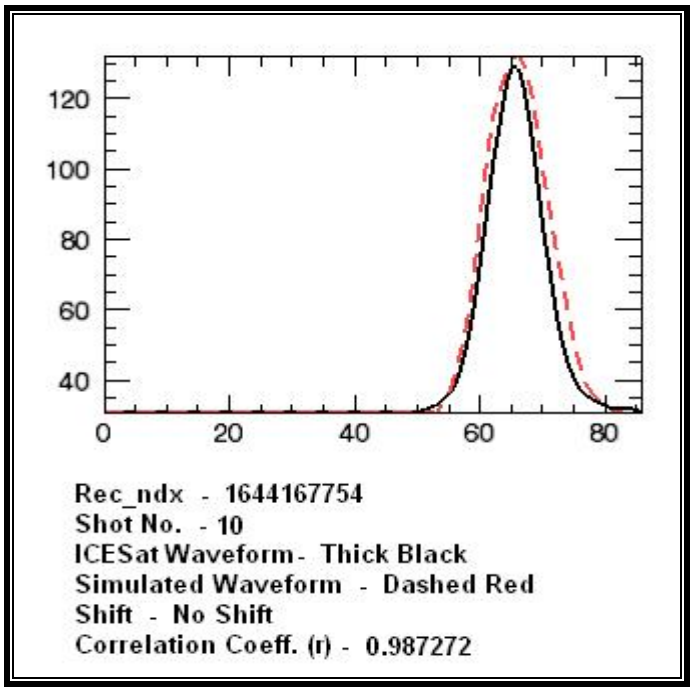

Figure 13 : Simulated waveform (dashed red) and ICESat waveform (black)over flat terrain

5.2.2. Simulation results over Gent ly Sloping Agricultural Land

5.2.2.1. Within footprint terrain characteristics

The footprint no. 1644167754_04 was analysed, this footprint is over the gently sloping agricultural land. Within footprint terrain slope is between 3°-5°. The standard deviation of within footprint heights is 0.514105. The Field observation shows that two crops are commonly cultivated in the fields. One is a variety of Red Gram or Pigeon Pea. A very famous pulse in India called Rahar or Arhar or Toor Dal. And the other one is Millet or Bajra (in India). The height of the fully grown Arhar & Millet crops is around 1.5 – 2.5 m. (Figure 14). As per the information from local farmers the Pigeon Pea crop is usually cultivated from July to March and Millet is usually cultivated in period from July to October.

Figure 14 : Red Gram crop i n its half grown stage.

5.2.2.2. Simulated waveform

The ICESat recorded waveform over gently sloping agricultural field is given in Figure 15. It shows several modes in the curve. These peaks are very near to each other.

Full-waveform was simulated using the CARTOSAT DEM, over gently sloping terrain. The simulated waveform is single modal curve (Figure 15). It matches with the ICESat waveform in the beginning of the signal or with the first mode of the waveform.

The Pearson's correlation coefficient between ICESat and simulated waveform is high with value of R = 0.873233.

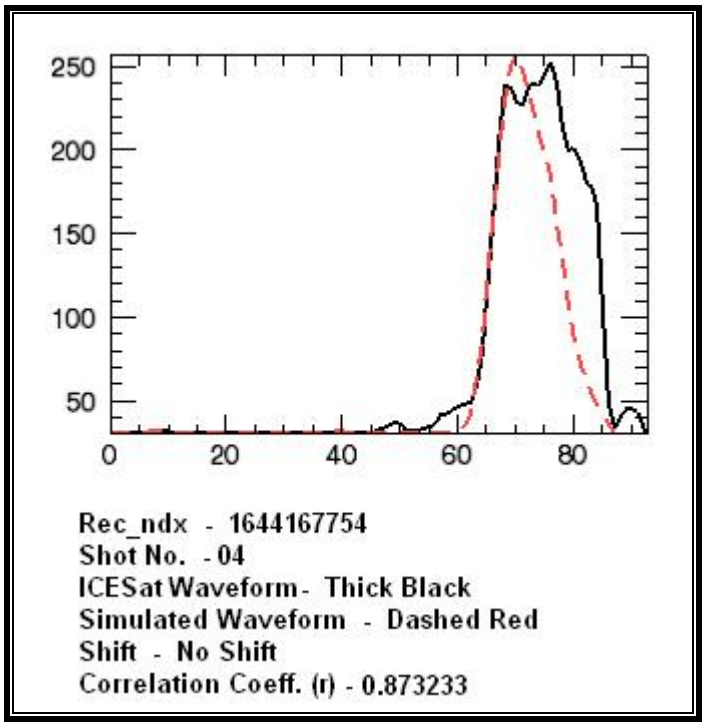

Figure 15 : Simulated waveform (dashed red) and ICESat waveform (black) over gently sloping agricultural field

5.2.2.3. Discussion on the simulation results

The ICESat data is acquired on 17th March 2008 during L3j campaign. And the CARTOSAT stereo images are acquired on 27th September 2006. During the field work, interaction with farmers revealed that in March/April the red gram crop is fully grown in the fields, and in September/October millet is fully grown in fields. Both the crops attain the height around 2 – 2.5 m. When it is fully grown, canopy top will be quite dense. Therefore CARTOSAT DEM appears to represent the top of crop canopy, whereas looking to the ICESat waveform it appears that it has penetrated to the crop canopy and recorded its vertical distribution.

The very nearly situated modes of the ICESat recorded waveform is due to the mixing of crop and ground returns in the gently sloping terrain. The ICESat data is of March and the Red Gram crop in the field is at its max height at that time. The signals from the crop and ground are mixed to form this type of complex waveform.

The single mode in the simulated waveform is due to the reference DEM. The CARTOSAT DEM represents only the top surface of the crop canopy, which is more or less flat. CARTOSAT DEM could not represent the vertical distribution within the crop canopy. Therefore it generates single modal waveform. Whereas the ICESat Laser beam

is penetrated into the crop canopy and showing multimodal curve. This is also the reason why simulated waveform matches more with the signal beginning part of the ICESat waveform.

A very gentle slope of around 3°-5° may also contribute to the widening in the ICESat waveform The base of both the waveforms is similar this shows that ICESat and CARTOSAT both are capturing the slope of terrain.

5.2.3. Simulation results over High Sloping Terrain

5.2.3.1. Within footprint terrain characteristics

Footprint 1644167754_1 was analysed for the high sloping terrain. The length of slope is approximately 150 m. towards south direction, and the footprint is situated in the middle part of the sloping surface (Figure 16). The slope within footprint is between 45° - 65° and it is continuous within the footprint. The standard deviation of within footprint heights is 11.6022. The standard deviation was calculated using the within footprint DEM elevations. The slope is very steep and fractured rock blocks and small shrubs are present on the slope.

Figure 16 : Terrestrial snapshot of the large slope with approximate location of footprint over sloping terrain (red ellipse).

5.2.3.2. Simulated waveform

The ICESat waveform of footprint 1644167754_01 is shown in the Figure 17 with thick black curve. This waveform is multi modal with combinations of many Gaussian components. It shows wider base because of the large slope within footprint. Multi modal nature of the waveform is depicting that there are several dominant reflecting surfaces within the slope.

The waveform was simulated using the developed algorithm (Figure 17). Pearson's correlation coefficient was calculated between ICESat waveform and simulated waveform and the result show the correlation value as 0.660186, which is low.

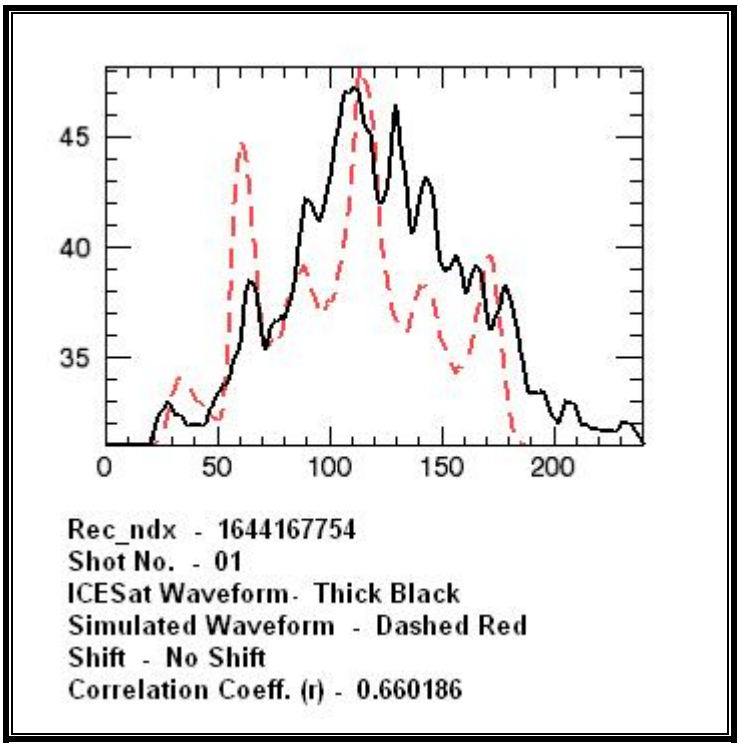

Figure 17 : Simulated waveform (dashed red) and ICESat waveform (black) over High sloping terrain.

5.2.3.3. Discussion on the simulation results

The simulated waveform and ICESat waveforms are not matching well. The ICESat waveform is showing more number of peaks in the curve. Simulated waveform shows less number of peaks in the curve. This difference between both waveforms can be caused by presence of the shrubs in the slope or the footprint geolocation errors. The small vegetation present in the sloping terrain increases the amount of backscatter laser energy at some elevation levels, which is evident by the higher peak in the ICESat waveforms compared to the simulated waveform. In the simulated waveform CARTOSAT DEM, which is generated at 2.5 m grid, is not able to capture small relief

variations in the terrain due to the presence of small vegetation. Therefore the simulated waveform has less number of peaks in the curve.

This waveform was generated without any shift in footprint geolocation. Error in the footprint geolocation can also cause some changes in the waveforms because the terrain relief is highly variable.

5.2.4. Simulation results over Highly Rugged Ravine topography

5.2.4.1. Within footprint terrain characteristics

The footprint ID 1644167754_20 was analysed for ravine topography. This footprint is over dense ravine area (Figure 18). Field measurements show that within footprint ravines is 12-14 m deep. The top levels of the ravines are very narrow and with very steep slope around 60° - 75°. The intermediate level consists of secondary ravines with 6 – 8 m height from the base with slope between 60° - 40°. The base level of ravines is sloping with 15° - 25°. The ravines within the footprint are U-Shaped with the width of around 10 -15 m. Standard deviation of within footprint heights is 2.85767. The footprint does not have vegetation, only a few small thorn shrubs are present.

Figure 18 : Ravines near GLAS footprint

5.2.4.2. Reference DEM

The full-waveform simulated over ravine terrain was not matching well with the ICESat waveform, because the input DEM was not well representing the very high variability of ravine terrain. Therefore the reference DEM generated by CARTOSAT stereo imagery over ravines, was enhanced by including the field measurements. The field measurements of within footprint ravine were taken using DGPS and Laser distance meter with high accuracy. These observations were included into the CARTOSAT DEM. The result of the refinement of the reference DEM is given in Figure 19. Unrefined DEM to the left in the Figure 19 is showing generalized relief of ravines whereas refined DEM is better representing highly rugged terrain of ravine.

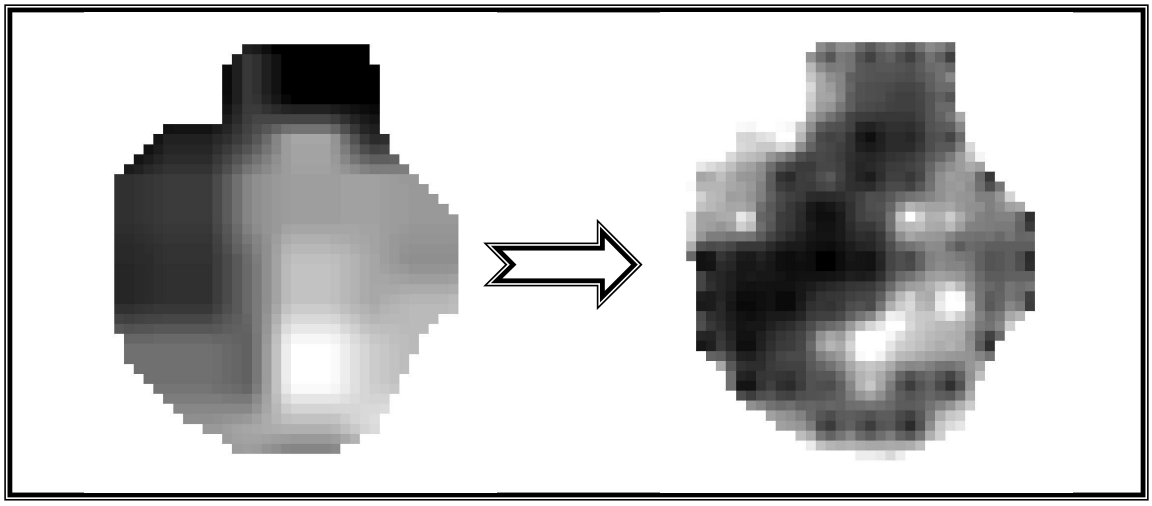

Figure 19 : Within footprint CARTOSAT DEM over ravines at 2.5 m pixel resolution without refinement (left), and after refinement (right).

5.2.4.3. Simulated waveform

ICESat waveform over the ravenous terrain shows multi-modal curve (Figure 20). The waveform shows mainly three types of returns, which represent three levels of the ravine structure. The signal beginning part shows weak signals, middle part of the waveform is showing strong returns with highest peak and the signal ending part of the waveform shows moderate returns.

Simulation of waveform over the ravine terrain was done using the refined DEM. Simulated waveform shows good correlation with the ICESat waveform (Figure 20). The pearson's correlation coefficient value is 0.809681 It also shows three different components, signal beginning part, middle part and the signal ending part. In simulated waveform signal beginning part shows good returns, middle part is very high with highest peak and the signal ending part also shows good returns.

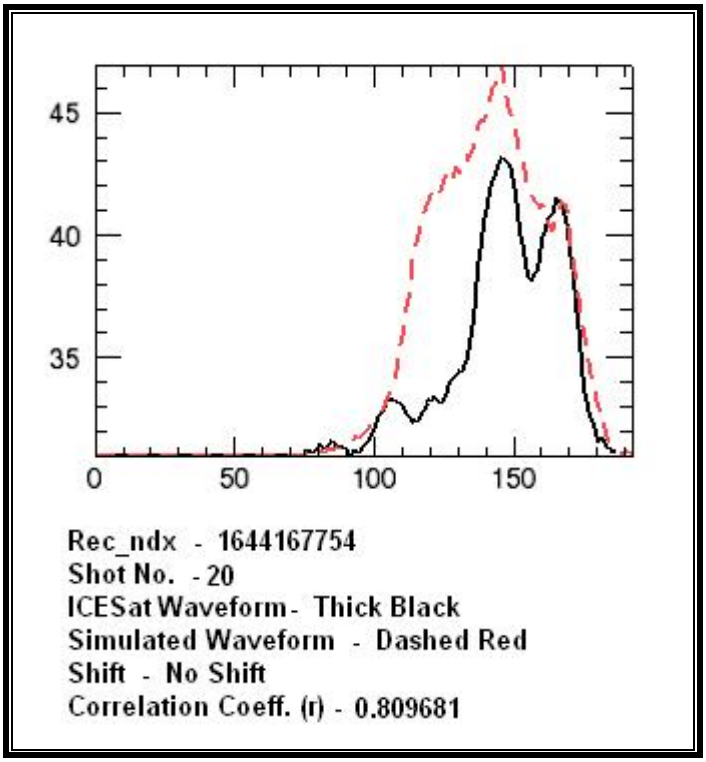

Figure 20 : Simulated waveform (dashed red) and ICESat waveform (thick black) over ravine terrain.

5.2.4.4. Discussion on the simulation results

ICESat waveform and simulated waveform both were representing three main levels of the within footprint ravines. The signal beginning part was representing the top levels of the ravines with height between 12 - 15 m. The top level of the ravine is very narrow (< 2 m) and very steep sided, with sloping angles between 60° - 75°. Due to the narrowness and steepness of the top of ravines, backscattered laser signals were weak in the ICESat recorded waveform. Whereas in the case of simulated waveform, reference DEM was used, in which the ravine top level was a bit wider and flat because of the interpolation and the pixel size. During the refinement of the DEM, measurement samples in all the levels of the ravines were considered and interpolation was done into 2.5 m grid. Due to this, very high relief variations on the top of ravine are generalized in the reference DEM. This caused an increase in amount of backscattered signals in simulated waveform.

5.3. Geolocation accuracy assesment

In this study, footprint geolocation accuracy was assessed for the footprint over the high sloping terrain. Footprint 1644167754_1 was analysed for the footprint geolocation accuracy. The LPA image of the footprint was shifted 5 m, 7.5 m, 10 m & 15 m around the original footprint location, towards North, East, South, and West.

Waveform was re-simulated after shifting LPA over DEM. Then correlation coefficient between simulated waveform and ICESat waveform is derived for each shift. The shifts and its correlation coefficients are given in Table 5.

Table 5 : Correlation analysis of the Geolocation accuracy of the GLAS footprint

Shift	North	*South*	East	West
5 m	0.523006	0.730967	0.626824	0.479598
7.5 m	-	***0.804606***	-	-
10 m	0.443196	0.765105	0.671296	0.634938
15 m	-	0.749920	-	-

The correlation coefficient for southern shift is more compared to shifts towards other directions. Shift of 7.5 m towards the south direction is showing maximum correlation (R = 0.804606) between the simulated waveform and ICESat waveform. Correlation results show that the shift towards south and East are increasing. Therefore shift towards South-East (SE) and South South-East (SSE) was also analysed. The correlation coefficient value of 7 m shift towards South-East was 0.712941, and 9 m shift towards South South-East was 0.770843. Simulated waveforms after footprint shift are given in the Figure 21.

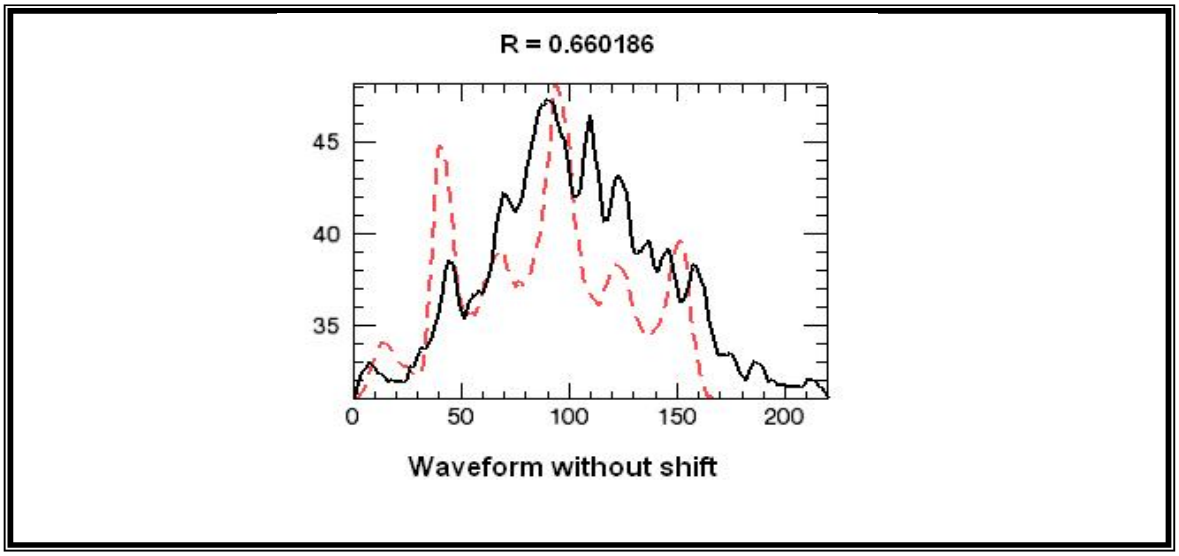

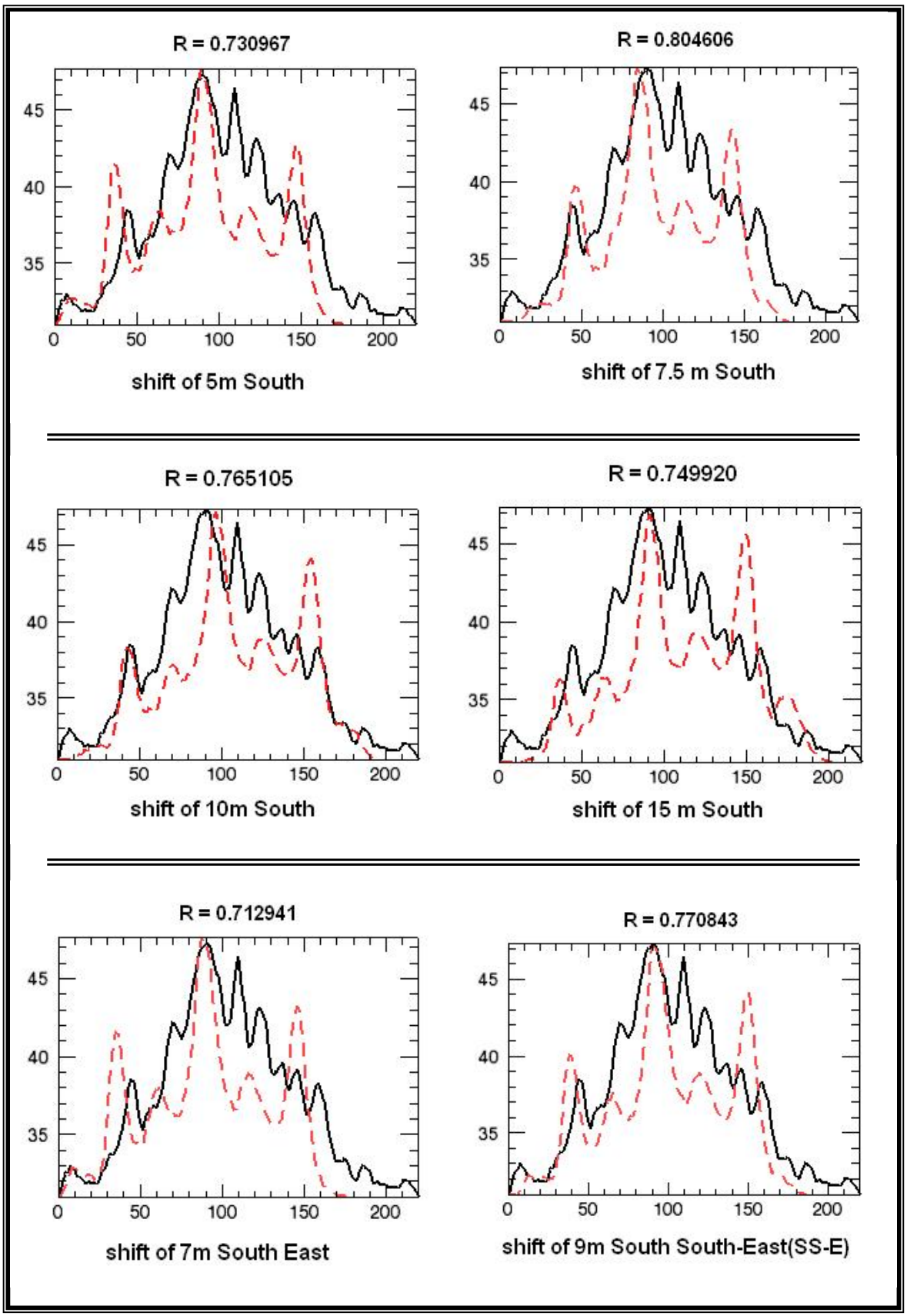
R = 0.730967
shift of 5m South
R = 0.804606
shift of 7.5 m South
R = 0.765105
shift of 10m South
R = 0.749920
shift of 15 m South
R = 0.712941
shift of 7m South East
R = 0.770843
shift of 9m South South-East(SS-E)

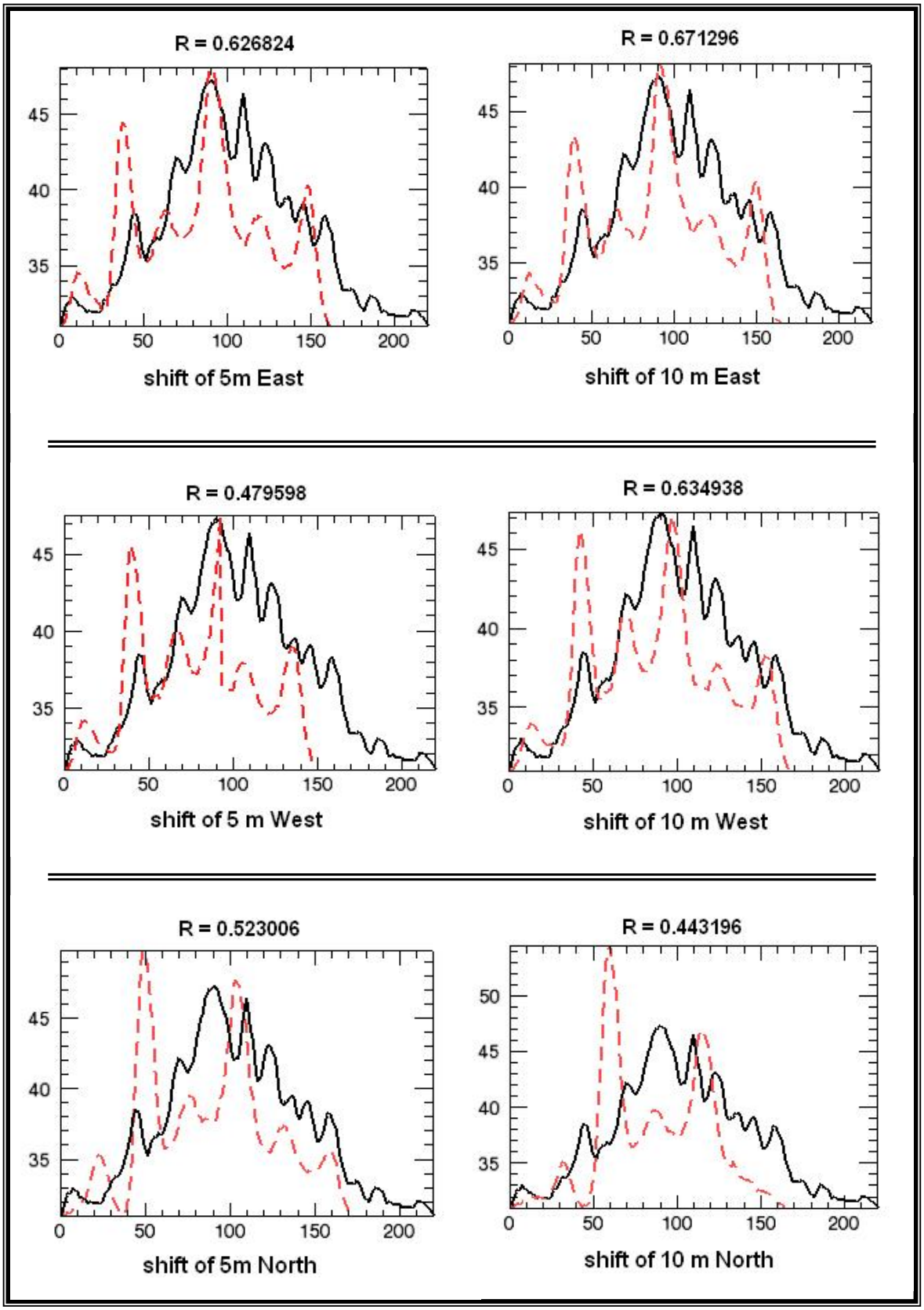

Figure 21 : Simulated waveforms after footprint shift

Similarly, footprint no. 1644167754_20 over ravine terrain was also analysed for geolocation accuracy. The footprint was shifted by 7.5 m towards south and waveform was simulated. The result of the simulation is given in Figure 22. The results shows that the correlation between the simulated waveform and ICESat waveform have increased from 0.809681 (without footprint shift) to 0.851955 (after footprint shift) by shifting the footprint 7.5 m towards South.

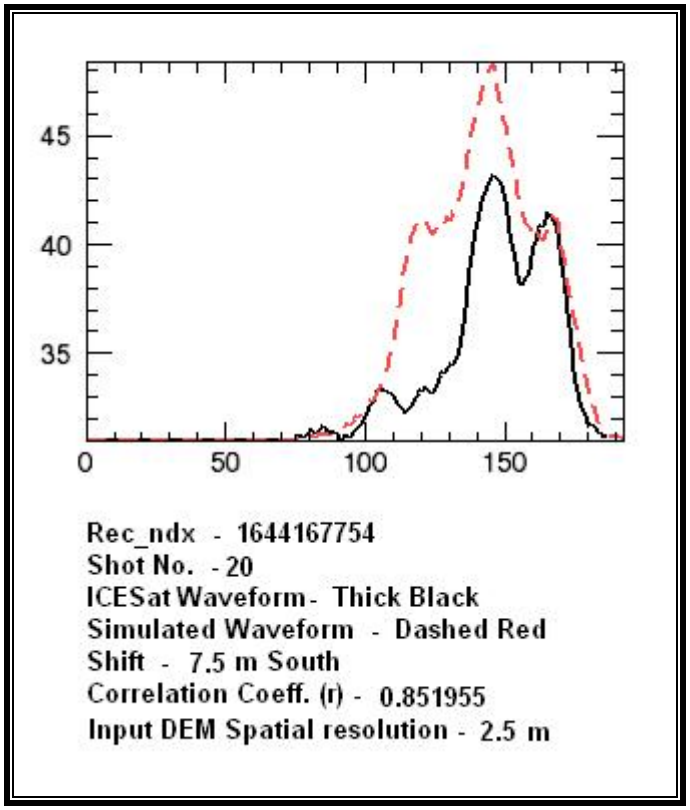

Figure 22 : Simulated waveform after shifting footprint by 7.5 m towards South (dashed red) and ICESat waveform (black) over ravine terrain.

5.4. Factors affecting the simulation results

From the comparative analysis of simulated to observed waveform, the differences between them could be attributed to four main factors: the Reference DEM resolution and accuracy, Vegetation cover of the terrain, Geolocation accuracy in the footprint and Reflectance characteristics of within footprint terrain.

Reference DEM: - The results of the waveform simulation depend a lot on the reference DEM. When simulating the waveform over rouged terrain, the spatial resolution and accuracy of the reference DEM plays a major role. It was observed that when the input reference DEM was resampled to 1 m grid, the simulated waveform

showed more correlation with the ICESat waveform (Figure 23). The correlation was increased from 0.851955 to 0.908011. In the resulted waveform, signals from the top of ravines are slightly reduced compared to the simulated waveform from 2.5 m grid DEM.

In the ravine terrain inside footprint, the top of ravines are very narrow (< 2 m) and with very high sloping faces (60° - 75°). This is the reason why ICESat recorded energy is less for the ravine top. In the case of 2.5 m grid DEM the narrow ravine top level is generalized which resulted into strong signals from top levels in simulated waveform. When the input reference DEM was interpolated into 1 m grid the relief variations were better represented, hence the simulated waveform shows more correlation with the ICESat waveform.

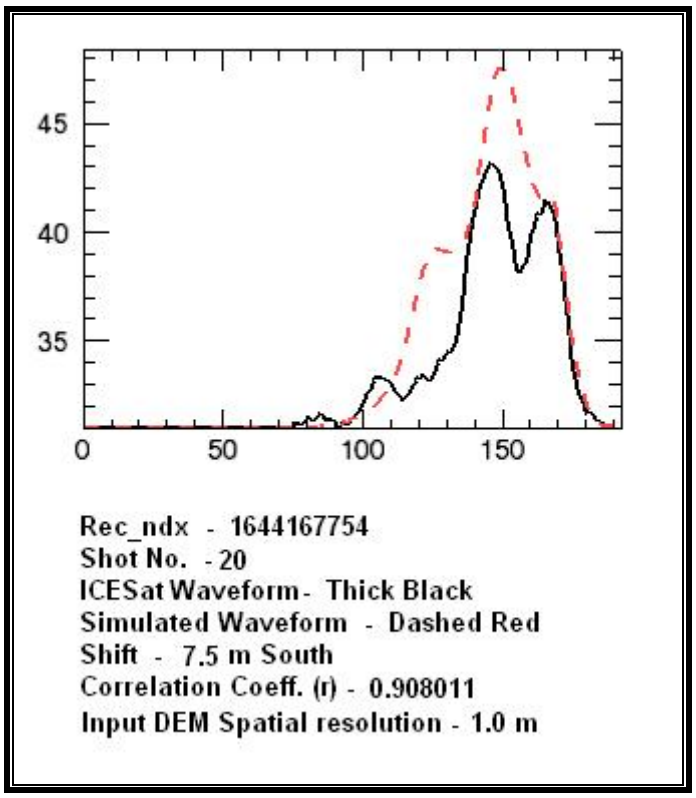

Figure 23 : Simulated waveform after interpolating into 1 m grid and shifting footprint by 7.5 m towards South (dashed red) and ICESat waveform (black) over ravine terrain.

The accuracy of the input reference DEM also affected the simulated results. When minor terrain relief was not well recorded in the DEM, the resultant simulated waveform showed lack of matching with the ICESat waveform. The simulated waveform without DEM refinement showed less matching with the ICESat waveform.

When the DEM was refined by including the field measurements with DGPS & laser distance meter, the matching of the waveform was increased.

Small Shrubs & Vegetation: - small shrubs present within the footprint will also cause the differences in the simulated waveform and ICESat waveform. Shrubs were not penetrated by the optical CARTOSAT DEM, it represented the top surface of the small vegetation. Therefore the simulated waveform of footprint 1644167754_04, over gently sloping agricultural land, represented the top of crop canopy surface. ICESat laser energy penetrated through the small vegetation; hence it showed slightly different waveform, compared to the simulated waveform.

Sensor Characteristics & Terrain reflectance: - The sensitivity of the recorder in ICESat and reflectance of various ground objects for 1064nm wavelength, will also play a major role in causing the differences between the ICESat waveform and simulated waveform. The intensity of the backscattered laser energy will be affected by the terrain roughness and slope. Backscattered laser energy will be different for different amount of terrain slope. Form high sloping terrain less energy will backscatter. The effect of the slope in the backscattered laser energy is not included in this algorithm.

Atmospheric effects and noise: - atmospheric conditions at the time of data acquisition may also cause the difference in the simulated waveform and ICESat waveform, because these factors are not included in the simulation algorithm.

6. Conclusions & Recommendations

6.1. Conclusion

The main aim of this research work was to analyse the ICESat full-waveforms over highly rugged topography, in particular ravines. An attempt was made to develop a simulation algorithm to generate model ICESat waveforms. Simulated waveforms showed high correlation coefficients for flat terrain. Results from the simulation algorithm shows that the developed algorithm performs well over rugged terrain. By simulation of the waveform understanding about the behaviour of the ICESat waveforms over rugged topography can be developed. It shows that the ICESat waveform represent the terrain relief variations very well over such a highly rugged terrain of ravines.

A new method of georeferencing the LPA image for better visualization of the footprint over terrain is developed. The georeferenced LPA images provide better footprint geometry and shape on the ground. It can be visualised over the Google Earth or any other georeferenced imagery, by which better understanding can be developed about within footprint terrain features. The georeferenced LPA images were also used to estimate the geolocation errors in the footprint of the ICESat.

6.2. Answers to research questions

1. What parameters will be required to simulate the ICESat full-waveform over highly rugged terrain?

In the simulation algorithm spatial and temporal distribution of the transmitted laser beam, and within footprint terrain variations, were required. In this research spatial distribution of the transmitted laser beam was derived by the georeferenced LPA image of the footprint. Temporal distribution was derived by digitized waveform of the transmitted laser pulse. The within footprint terrain was represented by the reference CARTOSAT DEM. The DEM was further refined by including the field measurements of the ravines using DGPS & Laser distance meter. Waveforms simulated using CARTOSAT DEM show good results for the flat terrain and uniformly sloping terrain. Over rugged terrain, spatial resolution of the reference DEM affects the simulation results. When the spatial resolution of the input DEM was

changed from 2.5m to 1m simulated waveform showed increase in the correlation with ICESat waveform.

2. How to georeference the LPA images to get better visualization of the ICESat footprints over terrain?

The LPA images were found very useful to identify the within footprint spatial distribution and the shape & size of the laser beam footprint. A new method is developed to georeference the LPA images to get better visualization of the ICESat footprint on the ground. To georeference LPA images, footprint range and coordinates information given in the GLA14 data product was required. Using the range information spatial resolution of the LPA is calculated. The average spatial resolution of the LPA was 10.4 m. Footprint coordinates was used to calculate GCP for georeferencing of LPA images.

For better visualization of ICESat footprints, LPA images were georeferenced and converted to KML. These KML files of the ICESat footprint LPA were visualized over Google Earth. This visualization of the ICESat provided better analysis of the footprint shape, size, and illuminated features within footprint. Georeferenced LPA images can easily be overlaid on georeferenced satellite imagery as well to get better visualization of the ICESat footprint.

3. How well the actual ICESat full-waveform can be represented by simulated waveform over different terrains?

Full-waveform of ICESat was simulated over terrain with different ruggedness. Simulation algorithm showed very high correlation coefficient over flat terrain. Over the rugged terrain the results of the simulation depends upon the Reference DEM resolution and accuracy, Vegetation cover of the terrain, Geolocation accuracy in the footprint and Reflectance characteristics of within footprint terrain. Refining the reference DEM by including field measurements improved the correlation between the simulated waveforms and original waveforms. Changing the spatial resolution of the reference DEM also improved the correlation between the waveforms. Geolocation accuracy of the ICESat footprint also affects the simulation results. Over the flat terrain shifting the footprint location will not change the shape of the waveform due to homogenous nature of the terrain. Whereas over the rugged terrain even a small shift 7.5 m in the footprint location improved the correlation between the ICESat waveform and simulated waveform.

4. How the ICESat full-waveform behaves over different terrain?

ICESat waveforms were classified according to within footprint terrain characteristics. Waveforms over flat barren land showed simple Gaussian nature and narrow width. Waveform over rugged topography showed complex nature with

multiple peaks and broad width. Over the ravine topography ICESat waveforms showed weak signals from the top level of the ravine due to the narrowness and steepness of the ravine top. By comparing the simulated waveform with the ICESat waveform it is interpreted that the ICESat waveform captured finer relief variations of ravine terrain than CARTOSAT DEM. Because the correlation between ICESat waveform and simulated waveform increased when spatial resolution of the reference DEM was reduced. Over the agricultural fields ICESat waveforms have penetrated the crop recorded the signals from crop canopy. The ICESat waveform over crop showed the multimodal curve, whereas the simulated waveform showed simple Gaussian curve. The simulated curve matched with the signal beginning of the ICESat curve which represents the top of crop canopy. CARTOSAT DEM was used for the simulation of waveform, which represented the top of crop canopy due to its optical nature. It shows that the ICESat waveform is recording signals from the crop canopy as well.

6.3. Recommendations

The georeferenced LPA images provide better estimations of the shape, size and illuminated features within ICESat footprint. Georeferenced LPA images are very useful for better visualization of the ICESat footprint over terrain. The automation of the georeferencing process of LPA will be very useful to quickly visualize the ICESat footprint.

Different types of objects within the laser illuminated area have different reflectance and scattering properties. To improve the simulation results these parameters can also be included in the algorithm. The slope of the terrain will also affect the intensity of backscattered laser energy from highly rugged terrain. Including the terrain slope for backscattering factor into the algorithm is expected to improve simulation results.

Simulation of waveform over highly rugged dense vegetated terrain will provide better understanding and analysis of the mixed signals from the vegetation canopy and the terrain.

In this study CARTOSAT DEM was used as the reference DEM for the simulation of full-waveform. The minor relief variations of the ravine topography were not well represented in the CARTOSAT DEM. This causes some differences between the simulated waveform and ICESat waveform. The simulation results can be improved by using more accurate and detailed DEM.

Reference:

Abshire J.B., McGarry J.F., Pacini L.K., Blair J.B., Elman G.C.; 1994; Laser Altimetry Simulator, Version 3.0 User's Guide; NASA Technical Memorandum, NASA/GSFC, Greenbelt, MD.

Abshire J.B., Sun X., Riris H., Sirota M.J., McGarry J.F., Palm S., Yi D., Liiva P.; 2005; Geoscience Laser Altimeter System (GLAS) on the ICESat Mission: On-orbit measurement performance; Geophysical Research Letters, 32, doi:10.1029/2005GL024028.

Anderson J., Martin M., Smith M.L., Dubayah R., Hofton M., Hyde P., Peterson B., Blair J., Knox R.; 2006; The use of waveform lidar to measure northern temperate mixed conifer and deciduous forest structure in New Hampshire; Remote Sensing of Environment, 105(3): 248 – 261.

Bae S., Schutz B.E.; 2002; Precision Attitude Determination; Geoscience Laser Altimeter System (GLAS); Algorithm Theoretical Basis Document (ATBD), version 2.2.

Blair J.B., Hofton M.A.; 1999; Modeling laser altimeter return waveforms over complex vegetation using high-resolution elevation data; Geophysical Research Letters, 26(16): 2509-2512.

Brenner A., Zwally H., Bently C., Csatho B., Harding D., Hofton M., Minister B., Robert L., Saba J., Thomas R., Yi D.; 2003; Derivation of range and range distribution from laser pulse waveform analysis for surface elevation, roughness, slope, & vegetation heights, Technical report GLAS, Algorithm theoretical Basis Document, version 4.1; http://www.csr.utexas.edu/glas/pdf/atbd_20031224.pdf (accessed on 6 February 2009).

Brenner A., Barbieri K., DiMarzio J., Gierber J., Robert L.A., Santana J., Sidel T.; 2008; Visualization software user's guide, Ver. 200807.0; http://nsidc.org/data/icesat/tools.html (accessed on 20 February 2009).

Chatterjee R.S., Saha S.K., Kumar S., Mathew S., Lakhera R.C., Dadhwal V.K.; 2009; Interferometric SAR for characterization of ravines as a function of their density, depth, and surface cover; ISPRS Journal of Photogrammetry and Remote Sensing, In press.

Drake J., Dubayah R., Clark D., Knox R., Blair J., Hofton M., Chazdon R., Weishampel J., Prince S.; 2002; Estimation of Tropical forest structural characteristics using large-footprint lidar; Remote Sensing of Environment, 79(2-3): 305 – 319.

Dubayah R., Blair J.; 2000; Lidar remote sensing for forestry applications; Journal of Forestry, 98(6): 44-46.

Duncanson L.I., Niemann K.O., Wulder M.A.; 2009; Estimating forest canopy height and terrain relief from GLAS waveform metrics; Remote Sensing of Environment, in press.

Gardner C.S.; 1992; Ranging performance of satellite laser altimeters; IEEE Transactions on Geoscience and Remote Sensing, 30(5): 1061-1072.

Geophysical Research Letters; 2005; Special issue on results from Ice, Cloud and land Elevation Satellite (ICESat) Mission; Geophysical Research Letters, 57.

Harding D.J., Carabajal C.C.; 2005; ICESat waveform measurement of within footprint topographic relief and vegetation vertical structure; Geophysical Research Letters, 32, doi: 10.1029/2005GL023471.

Hofton M., Minister J., Blair J.; 2000; Decomposition of laser altimeter waveforms; IEEE transactions on Geoscience and Remote Sensing, 38 (4): 1989–1996.

Hyde P., Dubayah R., Peterson B., Blair J., Hofton M., Hunsaker C., Knox R., Walker W.; 2005; mapping forest structure for wildlife habitat analysis using waveform lidar: Validation of montane ecosystems. Remote Sensing of Environment, 96(3-4): 427 – 437.

Mallet C., Bretar F.; 2009; Full Waveform Topographic Lidar: State-of-the-art; ISPRS Journal of Photogrammetry and Remote Sensing 64(1): 1-16.

National Snow and Ice Data Center, Data summaries. Available online at http://nsidc.org/data/icesat/data.html (accessed on 14 January 2009).

Pankaj Kumar; 2007; Dynamic Information Extraction for Rugged Topography from Multi Sensor Satellite Data; M.Sc. thesis, ITC-IIRS JEP, Dehradun.

Rim H.J., Schutz B.E.; 2002; Precision Orbit Determination (POD); Geoscience Laser Altimeter System (GLAS), Algorithm Theoretical Basis Document (ATBD), version 2.2.

Schutz B.E.; 2002; Laser Footprint Location (Geolocation) and Surface Profiles; Geoscience Laser Altimeter System (GLAS), Algorithm Theoretical Basis Document (ATBD), version 3.

Sharma H.S.; 1979; The Physiography of Lower Chambal valley and its Agricultural Development; Concept Pub. Co., New Delhi.

Sirota M.J., Bae S., Miller P., Mostofi D., Webb C., Schutz B., Luthcke S.; 2005; The transmitter pointing determination in the Geoscience Laser Altimeter System; Geophysical Research Letters, 32, doi:10.1029/2005GL024005.

Sun G., Ranson K.J.; 2000; Modeling Lidar Returns from Forest Canopies; IEEE Transactions on Geoscience and Remote Sensing, 38(6): 2617-2626.

Sun G., Ranson K.J., Kimes D.S., Blair J.B., Kovacs K.; 2008; Forest vertical structure from GLAS: An elevation using LVIS and SRTM data; Remote Sensing of Environment 112: 107-117.

Thiel K., Wehr A.; 2004; Performance and capabilities of laser scanner – an overview and measurement principle analysis; International Archive of Photogrammetry, Remote Sensing and Spatial Information Sciences, 36 (part 8/W2): 14-18.

Vosselman G., Mass H.-G.; 2009; Airborne and Terrestrial Laser Scanning; Whittless Publishing.

Yong P., Zangyuan L., Lefsky M., Sun G., Xinfang Y.; 2006; Model Based Terrain Effect Analyses on ICESat GLAS Waveforms; Geoscience And Remote Sensing Symposium, IGARSS-2006, doi: 10.1109/IGARSS.2006.830

Zwally H., Schutz B., Abdalati W., Abshire J., Bently C., Brenner A., Bufton J., Dezio J., hancock D., Harding D., Herrind T., Minister B., Quinon K., Palm S., Spinhirue J., Thomas R.; 2002; ICESat laser measurements of polar Ice, Atmosphere, Ocean, and Land; Journal of Geodynamics, 34(3): 405-445.

Appendices:

Appendix A : - Details of ICESat Laser Operation campaigns.

Laser campaign ID	Orbit ref. ID	Start date	End date	No. of days in campaign	Duration of repeat orbit	No. of repeat orbits	Footprint major axis mean & st. dev. (m)	Footprint eccentricity mean & st. dev.
Laser 2a	2103	13 Oct 2003	19 Nov 2003	38	91	0.40	105.3 ± 4.3	0.884 ± 0.012
Laser 2b	2107	17 Feb 2004	21 Mar 2004	34	91	0.36	89.8 ± 5.1	0.82 ± 0.05
Laser 2c	2107	18 May 2004	21 Jun 2004	35	91	0.38	88.4 ± 19.1	0.892 ± 0.044
Laser 3a	2109	3 Oct 2004	8 Nov 2004	37	91	0.39	55.8 ± 0.4	0.57 ± 0.04
Laser 3b	2111	17 Feb 2005	24 Mar 2005	36	91	0.39	79.3 ± 11.6	0.75 ± 0.05
Laser 3c	2111	20 May 2005	23 Jun 2005	35	91	0.37	55.4 ± 1.8	0.63 ± 0.03
Laser 3d	2113	21 Oct 2005	24 Nov 2005	35	91	0.36	52.0 ± 1.1	0.52 ± 0.01
Laser 3e	2115	22 Feb 2006	28 Mar 2006	34	91	0.37	52.3 ± 1.6	0.483 ± 0.04
Laser 3f	2115	24 May 2006	26 Jun 2006	33	91	0.36	51.2 ± 1.7	0.479 ± 0.025
Laser 3g	2117	25 Oct 2006	27 Nov 2006	34	91	0.36	53.4 ± 1.5	0.51 ± 0.04
Laser 3h	2119	12 Mar 2007	14 Apr 2007	34	91	0.37	55.6 ± 0.5	0.52 ± 0.02
Laser 3i	2121	2 Oct 2007	5 Nov 2007	37	91	0.37	57.3 ± 0.6	0.59 ± 0.01
Laser 3j	2123	17 Feb 2008	21 Mar 2008	34	91	0.36	58.7 ± 0.6	0.52 ± 0.04

Appendix B : - Useful Product variables of GLA01 data product of ICESat.

Product Var Name	Short Description	Offset (Bytes)	Product Data Type	Total Bytes	Product Units	Product Minimum	Product Maximum
Record Type:GLA01_MAIN; Record Duration (seconds):1; Repeats: 1							
i_rec_ndx	GLAS Record Index	0	i4b	4	N/A	0	2147483647
i_UTCTime	Transmit Time of First Shot in frame in J2000	4	i4b (2)	8	seconds, microseconds	0	2147483647
i_gla01_rectype	GLA01 Record Type	12	i2b	2	n/a	0	2
i_dShotTime	Laser Shot Time Deltas (shots 2-40)	16	i4b (39)	156	microseconds	0	1200000
i1_pred_lat	Predicted geodetic Latitude of the laser footprint	172	i4b	4	microdegrees	-90000000	90000000
i1_pred_lon	Predicted geodetic Longitude of the laser footprint	176	i4b	4	microdegrees	0	360000000
i_RespEndTime	Ending Address of Range Reponse	180	i4b (40)	160	nanoseconds	0	5100000
i_LastThrXingT	Last Threshold Crossing Location for Selected Filter	340	i4b (40)	160	ns	0	5100000
i_NextThrXing	Next to Last Threshold Crossing Location for Selected Filter	500	i4b (40)	160	ns	0	5100000
i_EchoPeakLoc	Echo Peak Location	660	i4b (40)	160	nanoseconds	0	5100000
i_EchoPeakVal	Echo Peak Value	820	i2b (40)	80	counts	0	255
i_wt_fact_filt	Filter Weight Factors	900	i4b (6, 40)	960	unitless	0	2000000000
i_filtr_thresh	Selected Filter Threshold Value	1860	i2b (40)	80	counts	0	255
i_time_txWfPk	Transmit Pulse Peak Location	1940	i4b (40)	160	ns	0	500000
i_TxWfStart	Starting Address of Transmit Pulse Sample	2100	i4b (40)	160	ns	0	500000
i_TxNrg_EU	1064 nm Laser Transmit Energy	2260	i4b	4	microjoules	0	90000
i_RecNrgAll_EU	1064 Laser received Energy from all signal above threshold	2264	i4b (40)	160	attojoules	0	200000
i_RecNrgLast_EU	1064 nm Laser Received Energy (max pk)	2424	i4b (40)	160	attojoules	0	200000
i_tx_wf	Sampled Transmit Pulse Waveform	2714	i1b (48, 40)	1920	counts	0	255
Record Type:GLA01_LONG; Record Duration (seconds):0.2; Repeats: 5							
i_rec_ndx	GLAS Record Index	0	i4b	4	N/A	0	2147483647
i_UTCTime	Transmit Time of First Shot in frame in J2000	4	i4b (2)	8	seconds, microseconds	0	2147483647
i_gla01_rectype	GLA01 Record Type	12	i2b	2	n/a	0	2
i_shot_ctr	Shot Counter	24	i2b (8)	16	counts	0	200
i_rng_wf	1064 nm Range Waveform	176	i1b (544, 8)	4352	counts	0	255
i_rawPkHt	Height of Peak in Raw Waveform	4544	i1b (8)	8	n/a	0	255

Note : i1b = integer 1 bit, i2b = integer 2 bit, i4b = integer 4 bit.

Appendix C : - Useful Product variables of GLA04 data product of ICESat.

Product Var Name	Short Description	Offset (Bytes)	Product Data Type	Total Bytes	Product Units	Product Minimum	Product Maximum
Record Type:GLA04_LPA_MAIN; % of Granule: 100; Record Duration (seconds):1; Repeats: null							
i_rec_ndx	GLAS Record Index	0	i4b	4	N/A	0	2147483647
i_UTCTime	Transmit Time of First Shot in frame in J2000	4	i4b (2)	8	seconds, microseconds	0	2147483647
i_dShotTime	Laser Shot Time Deltas (shots 2-40)	12	i4b (39)	156	microseconds	0	1200000
i_shot_cntr	Shot Counter	168	i2b (40)	80	counts	0	200
i_GPSLatch	GPS Latch Time	248	i4b (2)	8	seconds, microseconds	null	null
i_boxX	X Position of Box	256	i1b (40)	40	counts	0	79
i_boxY	Y Position of Box	296	i1b (40)	40	counts	0	79
i_PixInt	LPA Data	336	i1b (400, 40)	16000	counts	0	255
i_tx_wf	Sampled Transmit Pulse Waveform	16336	i1b (48, 40)	1920	counts	0	255
i_time_txWfPk	Transmit Pulse Peak Location	18256	i4b (40)	160	ns	0	500000
i_TxWfStart	Starting Address of Transmit Pulse Sample	18416	i4b (40)	160	ns	0	500000
i_txWfPk_Flag	Transmit Waveform Peak Status Flag	18576	i1b (40)	40	n/a	0	8

Note : i1b = integer 1 bit, i2b = integer 2 bit, i4b = integer 4 bit.

Appendix D : - Useful Product variables of GLA14 data product of ICESat.

Product Var Name	Short Description	Offset (Bytes)	Product Data Type	Total Bytes	Product Units	Product Minimum	Product Maximum
Record Type:GLA14_MAIN; Record Duration (seconds):1; Repeats: 1							
i_rec_ndx	GLAS Record Index	0	i4b	4	N/A	0	2147483647
i_UTCTime	Transmit Time of First Shot in frame in J2000	4	i4b (2)	8	seconds, microseconds	0	2147483647
i_transtime	One way transit time	12	i2b	2	microseconds	0	4000
i_dShotTime	Laser Shot Time Deltas (shots 2-40)	20	i4b (39)	156	microseconds	0	1200000
i_lat	Coordinate Data, Latitude, specific to land range	176	i4b (40)	160	microdeg	-90000000	90000000
i_lon	Coordinate Data, Longitude, specific to land range	336	i4b (40)	160	microdeg	0	360000000
i_elev	Land surface Elevation	496	i4b (40)	160	mm	-500000	10000000
i_tpintensity_avg	Transmit Pulse intensity - frame avg	2664	i4b	4	counts	0	25500
i_tpazimuth_avg	Transmit Pulse azimuth - frame avg	2668	i2b	2	degrees*10	0	3600
i_tpeccentricity_avg	Transmit Pulse eccentricity - frame avg	2670	i2b	2	Unitless*1000	0	1000
i_tpmajoraxis_avg	Transmit Pulse major axis - frame avg	2672	i2b	2	cm	0	10000
i_DEM_elv	DEM Elevation	2792	i4b (40)	160	cm	-50000	1000000
i_refRng	Reference Range	2952	i4b (40)	160	mm	400000000	1000000000
i_ldRngOff	Land Range Offset	3272	i4b (40)	160	mm	-150000	0
i_reflctUncorr	Reflectivity not corrected for Atmospheric Effects	4552	i4b (40)	160	Unitless*1E06	0	1000000
i_reflCor_atm	Reflectivity Correction Factor For Atmospheric Effects	4712	i4b	4	Unitless*1E06	0	1000000
i_numPk	Number of Peaks found in the Return	4876	i1b (40)	40	N/A	0	6
i_kurt1	Kurtosis of Received Echo (alternative)	4916	i2b (40)	80	unitless * 100	-1000	1000
i_skew1	Skewness of Received Echo (alternative)	4996	i2b (40)	80	unitless * 100	-10000	10000
i_Gamp	Amplitudes of Gaussians	5236	i4b (6, 40)	960	0.01 volts	0	300
i_Garea	Area under Gaussian	6196	i4b (6, 40)	960	0.01 volts * ns	0	348457
i_Gsigma	Sigma of Gaussians	7156	i4b (6, 40)	960	0.001 ns	0	327660
i_erd	Estimated Range Delay	8242	i2b	2	Millimeters	0	1000
i_cld1_mswf	Cloud Multiple Scattering Warning Flag	8246	i1b	1	NA	0	15
i_rngCorrFlg	Range Correction Flag	8452	i1b (2)	2	N/A	0	32767
i_DEM_hires_elv	High Resolution Elevation	8508	i2b (40)	80	meters	-500	13000
i_RecNrgAll	Received Energy signal begin to signal end	8988	i2b (40)	80	0.01 fJoules	0	32000
i_Surface_temp	Surface Temperature	9428	i2b	2	degrees Celsius * 100	-10000	10000
i_Surface_pres	Surface Pressure	9430	i2b	2	millibars of mercury * 10	0	20000
i_Surface_relh	Relative Humidity	9432	i2b	2	percentage * 100	0	10000
i_maxRecAmp	Max Amplitude of Received Echo	9434	i2b (40)	80	Tenth of millivolts	-300	30000
i_sDevNsOb1	Standard deviation of 1064 nm Background noise	9514	i2b (40)	80	0.0001 volts	0	30000
i_TxNrg	1064 nm Laser Transmit Energy	9796	i2b (40)	80	0.01 millijoules	0	32766